CONSERVED-MASS METASTRUCTURES FOR VIBRATION SUPPRESSION

by

Ehab Emad Basta

A Thesis presented to the Faculty of the
American University of Sharjah
College of Engineering
In Partial Fulfillment
of the Requirements
for the Degree of

Master of Science in
Mechanical Engineering

Sharjah, United Arab Emirates

April 2019

Approval Signatures

We, the undersigned, approve the Master's Thesis of Ehab Emad Basta.

Thesis Title: Conserved-Mass Metastructures For Vibration Suppression

Signature	**Date of Signature** (dd/mm/yyyy)
Dr. Samir Emam Associate Professor, Department of Mechanical Engineering Thesis Advisor	
Dr. Mehdi Ghommem Assistant Professor, Department of Mechanical Engineering Thesis Co-Advisor	
Dr. Maen Alkhader Associate Professor, Department of Mechanical Engineering Thesis Committee Member	
Dr. Mohammad AlHamaydeh Associate Professor, Department of Civil Engineering Thesis Committee Member	
Dr. Mamoun Abdel-Hafez Head, Department of Mechanical Engineering	
Dr. Lotfi Romdhane Associate Dean for Graduate Affairs and Research	
Dr. Naif Darwish Acting Dean, College of Engineering	
Dr. Mohamed El-Tarhuni Vice Provost for Graduate Studies	

Acknowledgement

I would like first to thank my thesis advisors Dr. Samir Emam and Dr. Mehdi Ghommem in the Mechanical Engineering department at the American University of Sharjah for providing knowledge, guidance, support, and motivation throughout my research stages. The doors of my advisors' offices have been always open whenever I have a question about my research. I am deeply beholden for their great assistance, worthy discussion and suggestions.

I would like to thank the professors of the Mechanical Engineering department who taught me the master level courses with mighty teaching methods and skills. I really appreciate their dignified advices and motivation. I would like also to thank Dr. Maen Alkhader and Dr. Mohammad AlHamaydeh for accepting to serve in my thesis examining committee and their valuable discussions.

I am so grateful to the American University of Sharjah's graduate assistantship program for helping and providing the funding for the work.

Finally, I must express my profound gratitude to my parents for providing me with continuous encouragement throughout my years of study and through the process of researching and writing this thesis. This accomplishment would not have been possible without them. Thank you.

Dedication

To my family…

Abstract

Vibration suppression, cancellation or absorption is an expansive field of research, which has been the focus of numerous studies performed by scientists and engineers for decades. Metamaterials are a new class of semi-active composites that can be deployed to reduce vibration of the host structure (beam) within a desired frequency. In this thesis, we investigate the nonlinear vibrations of a metamaterial structure that consists of an Euler-Bernoulli beam host attached to a periodic array of spring-mass-damper subsystems deployed for vibration absorption. The governing equations of motion of the coupled system are derived and solved numerically. A mathematical model is first utilized to perform the linear free and forced vibration analyses. The effect of the local resonators on the suppression of the oscillations of the host beam is studied. The ability to mitigate the vibration of the host structure at a desired resonant frequency is achieved by tuning the resonant frequencies of the local absorbers. More interestingly, the results show that the simultaneous suppression of several modes is possible by tuning and properly placing each absorber along the host structure. More importantly, the results show that simply adding bulk mass to the host structure barely suppresses the vibration. The comparison between metastructure and adding bulk mass confirmed that the added mass using the metastructure assembly is essentially the reason for the mitigation and not the extra mass. Furthermore, the mathematical model is used to investigate the effect of the resonators (local absorbers) on the nonlinear behavior of the main structure when being subject to external forcing over an extended frequency range. The numerical study reveals that proper tuning of the local resonators allows significant vibration suppression of the metamaterial beam when being excited in the neighborhood of any of the first three natural frequencies. We demonstrate the capability of the metamaterial structure to withstand to external loading even when operating near resonance. Finally, we combine the nonlinear mathematical model with an optimizer to identify the number and tuning frequencies of the absorbers that maximize the vibration suppression. The optimization results show that significant mitigation can be achieved by tuning properly the absorbers in the vicinity of the host structure's natural frequencies.

Keywords: ***Metastructure; metamaterial; conserved-mass; local absorbers; nonlinear Dynamics; vibration suppression.***

Table of Contents

List of Figures

List of Tables

Chapter 1. Introduction

1.1. Overview

Vibration is the scope of dynamics which deals with repetitive motion of generally small amplitude. In our world, vibration is present almost everywhere. Vibrations range from the macro-scale such as the vibration of buildings or the vibration of a guitar string all through the micro-scale vibration such as the vibration of your vocal cords or the vibration of the human cells in the oncotripsy procedure [1] as an example. Vibration is desired in few cases such as in musical instruments and targeting of cancer cells using oncotripsy and can be exploited in some engineering applications such as filtering and sensing. Nevertheless, most of the applications require the suppression of the vibration as much as possible and remedy its effects. The periodic vibration of the wing of an aircraft will accumulate fatigue stress which in turn will cause failure. While building a bridge, the designer should account for avoiding frequencies of the external excitation to be equal to the natural frequency of the bridge. The aforementioned phenomenon is called resonance and this phenomenon causes drastic deflections and failure. Cars, aircrafts and even washing machines devices are equipped with devices which help in suppressing any kind of vibration for the comfort of the user. Thus, vibration, in most cases, needs to be mitigated by some way or another to avoid undesirable effects that may lead to the failure of the structure/system.

1.2. The Need to Mitigate Vibration

Control of vibration has been under constant research for the past years. Excess of vibration leads to the discomfort of the aircraft passengers for instance and moreover leads the aircraft itself to fatigue and fail. Generally, in vibration applications, numerous designs have been proposed and implemented to allow the minimal vibration possible. Most vibration mitigation techniques can be divided into active or passive systems. Active systems are where energy is required to control the vibration. Sensors and actuators that act against the vibration are examples of active systems. On the other hand, a passive vibration suppression system does not require any form of external energy. The suspension system of an automobile is an infamous example of such control. The suspension system of a car is based upon the passive vibration mitigation concept which is available in typical vibration reference books [62]. However, since this is a design process, there is not typically a unique solution for vibration mitigation.

1.3. Metamaterials

One of the proposed designs that has been the scope of research in the recent years is the concept of metamaterials. The term, metamaterial, is not widely spread in books but is gaining growing attention in recent literature. Being a recent topic, the history of this term is relatively easy to track.

The first metamaterial research started by studying the electromagnetic metamaterials which showed a negative permeability and/or permittivity [2,3]. In recent years, materials with negative permeability were experimentally established [4]. Metamaterials are man-made materials that behave differently from the nature of their own constituencies. In fact, this is what makes metamaterials special. Some unique properties to electromagnetic metamaterials are invisibility [5,6], negative refractive index [7] and inverse Doppler effect [8]. The aforementioned properties result purely from mechanically adjusting the material rather than affecting the material on a molecular level such as any chemical reactions applied on the material. For instance, the size, shape, alignment and prearrangement of the microstructure alter the transmission of light and create the unique, unusual material properties. Possible applications of such electromagnetic metamaterials are optical microscopes capable of observing atoms, artificial magnetic apparatus made of non-magnetic materials, photolithography for microfluidics applications, optical fibers with minimal transmission loss, photon tunneling, accurate image processing for biomedical applications, tracking on a cellular level, subwavelength waveguides and X-ray crystallography [9-11]. As an example, the conventional microscopes can look down as low as 400 nm, the limit of the visible light, which is a fraction of a red blood cell. On the other hand, optical super lenses which are electromagnetic metamaterials exhibit negative refractive index which enables the user to resolve images with a resolution which is almost one sixth of the wavelength of the visible light used in the conventional optical microscope [12]. The success of the electromagnetic metamaterials and their unique properties encourage researches to extend the metamaterial concepts to acoustic metamaterials [3, 13-19].

As mentioned before, electromagnetic metamaterials exhibit unusual properties in terms of permittivity and permeability just by altering the design of the material. Likewise, in acoustic metamaterials, subunits (resonators) can be designed to be

embedded with the host structure which is made of natural conventional material. These subunits locally resonate with the mechanical waves excited at the structure. This local resonance, exhibited by the mechanical subunits, result in material properties different from its constituents such as negative stiffness and negative effective mass [16-19, 20]. In short, acoustic metamaterials are artificial materials imbedded with internal microstructures to exhibit unusual properties such as negative modulus [21,22] and negative effective density [23,24]. This phenomenon is essentially the concept of acoustic metamaterial in particular. Fortunately, compared to the electromagnetic metamaterials, the manufacturing of acoustic metamaterials and their subunits is relatively easier. Nevertheless, modeling and simulating metamaterials is not easy because of their complex built-up composite structures. The utilization of these acoustic metamaterials is pronounced in metastructures that are proposed in the literature with few simple models [13-17, 19]. Notice that metastructures are the direct implementation of the metamaterials concept. In fact, the work presented in this thesis is mainly about the metastructure.

1.4. Metastructures

Metastructures or mechanical metamaterials, as stated in the preceding paragraph, are inspired by the metamaterial concept. Metastructures, in general, are the structures with distributed periodic vibration resonators. These structures are normal conventional structures integrated with a lattice or a periodic geometry of small absorbers. These periodic structures which are made up of an arrangement of absorbers are designed in a similar manner to show unique dynamic properties. These properties arise from their capability to function as mechanical filters for wave propagation. In the light of the preceding lines, one can define the metastructures as the structures integrated with localized resonant subunits for vibration damping. This wave damping is mainly due to the structural periodicity. Essentially, the periodicity is what makes these structures exhibit interesting dynamic characteristics which is worth the investigations in the literature.

Metastructures exhibit some interesting dynamic properties such as the bandgaps and pass bands. The local resonators suppress the vibration by allowing waves with certain frequency to propagate along the periodic subunits. These bands of frequency are called the ‘’Pass bands’’. On the other hand, these resonators block

certain waves with another set of frequencies to pass. This range of frequencies where propagation of waves is stopped or minimized are called “stop bands or bandgaps”. The stopbands can further be divided into Bragg-type bandgaps and resonant-type ones. The brag-type are practical for attenuating waves in the high frequency region. On the other hand, the locally resonant (LR) bandgaps is easier to manipulate and control [25-29]. It is the periodicity of the resonator which makes the stopband in action. Although the resonators might be made of non-dispersive materials, they still act as dispersive ones and prevent waves with a certain frequency (stopband) to propagate forward [20,30]. Speaking of bandgaps, wave propagation models are normally used to predict the stop bands in LR structures and represent the dispersive behavior of the wave. Some of these wave propagation models are the Transfer Matrix Method, Floquet models and Bloch-wave [31-34] In addition, Nouh *et al.* [48] uses the structural power flow approach to predict the stop bands. The structural power flow model is a mathematical tool which quantifies the transmission paths and energy flow in vibrating structures [35-41]. The band gap prediction is often represented as a part of the metastructure research. Some papers investigate the detailed analysis of the band gap prediction [55], whereas other papers concentrate on the actual working mechanism of the metastructure whether by mathematical models or finite element simulations or even experimental work.

1.5. Experimental and Simulation Work

Some of the relevant investigations done on 1D metastructures were conducted by Pai [46]. In [42], the author models a longitudinal host structure integrated with many small mass-spring absorbers. Xiao *et al.* [43] investigated an analogous structure to that used by Pai [46] but the absorbers have multiple degree of freedom. Xiao *et al.* concentrates on bandgap prediction and formation as well. Yu *et al.* [44] investigated the bending wave excitation on a metastructure beam embedded with many resonators. Chen *et al.* [45], had a similar model to Zhu but the host is a sandwich beam and the resonators are placed inside. Pai [46] studied the suppression of the longitudinal wave propagation and suggested metamastructures to be used for a broader mitigation of vibration. Liu [25] modeled a chiral latticed metastructure which proved to be functional for low-frequency vibration attenuation applications. Banerjee et al. [54] studied an impact-based mass-in-mass unit cell as a potential sub unit of a resonating metamaterial. Rather than beams, author such as Peng *et al.* [47] and Nouh *et al.* [48] studied metamaterial plates. Hu *et al.* [49] further investigated the possibility of

harvesting energy while suppressing the vibration of a metastructure. Very relevant to our work was the work done by Reichl and Inman [50] who studied and optimized a conserved-mass 1D metastructure model. Moreover, Casalotti *et al.* [51] investigated the effect of integrating nonlinear resonators to a structural metamaterial beam. The aforementioned studies mostly started with mathematical beam models. Some authors such as Chen *et al.* [52] and Pai *et al.* [53] used the extended Hamilton principle to obtain the equations of motion. Others used Newton's second law [50,54]. Moreover, these papers utilized well-known beam theories. For structural beams, the Euler-Bernouli beam and the Timoshkenko beam theory are the most used theories. Regarding the plates, Kirchoff's plate theory and Mindlin-Reissner plate theory are amongst the most used ones. A number of these studies validate their research further by employing a finite element model/package or performing an actual experiment.

A finite element model is usually developed to study the structural dynamics, frequency responses of metamaterial beams or plates embedded with an array of periodic local absorbers. Chen *et al.* [52] and Reichl *et al.* [50] used Abaqus [50,54] whereas Nouh *et al.* [48] and Harne *et al.* [55] used COMSOL Multiphysics. A few other researches introduced the challenging task of implementing an actual experiment on a built up metastructure. Chen *et al.* [52] presented experimental setup and results on a sandwich structure containing spring-mass absorbers. Maystre *et al.* [56] created one of the first metastructures. Calius *et al.* [57] verified that a silicone rubber coated steel ball in polymer resin matrix may function as a resonating subunit of the metastructure. The study showed that the steel ball acts as a resonating mass, the polymer matrix as an outer mass and the rubber coating as an internal spring. This was an overview of what has been done roughly on metastructures.

1.6. Conservation Of Mass

In light of the preceding sections, it is noticed that the previous work kept on adding the mass (resonators) to the host structure to keep the stiffness constant as in [58-60]. In our work, the mass is conserved which means that any added mass in the resonators are taken off the host structure itself. This is because mass and suppression are cross linked. Logically, one can increase the suppression capability of a host structure by simply adding mass to it. By conserving the mass, it is shown that the increased performance does not result from the additional mass. Our work aims at

showing that the altering of the dynamic properties occurs mainly due to the metastructure alignment and not due to any additional mass. Moreover, it is well known that an industry such as aerospace can save tons of money by minimizing the weight of the structure as much as possible.

1.7. Thesis Objective

The work of Reichl and Inman [50], Igusa and Xu [61], and Casalotti *et al.* [51] are all similar to the work done here in principle, but there are some important crucial differences. Igusa and Xu [61] used high levels of local damping in their subunits as a method of suppressing the vibration. Our work includes dampers for each absorber. However, these dampers are due to the internal damping of the absorbers and not external damping systems. It is the damping nature of the material of the absorbers. Moreover, their metastructure -with resonators – is heavier than the host structure without absorbers. Again, our work examines whether the suppression functionality comes from simply adding mass or the effect of the resonators. Reichl and Inman [50] used lumped conserved mass models but the metastructure are allowed to oscillate only longitudinally. Our work presented is interested in the flexural deformation, which is the case of many applications where beams are the host structure. The movement of the host structure and resonators occur in the vertical direction rather than the horizontal direction. Casalotti *et al.* [51] presented a metamaterial beam with integrated absorbers that can move in the vertical direction. Mass was not conserved, nevertheless. Moreover, the author takes the path of investigating the effect of the nonlinearity of the springs of the subunits on the assessment of the metastructure. In our work, the springs are modeled as linear springs and the optimization is performed essentially on linear vibration absorbers. The main contribution of this thesis is the integration of the optimizer which enables identifying the optimum tuning frequencies of the local absorbers for the maximum vibration suppression.

1.8. Research Contribution

The contributions of this research work can be summarized as follows:

- Propose a promising design on metastructures to mitigate multiple modes of a structural hinged-hinged beam in the linear regime
- Compare the effect of adding bulk mass to the host beam versus adding extra mass in the form of local periodic subunits

- Investigate the effect of the absorbers in the nonlinear regime and modulate the hardening effect in the neighbourhood of the first three modes
- Implement an optimization technique to maximize the reduction in the amplitude of vibrations while varying some control parameters

1.9. Thesis Organization

The rest of the thesis is organized as follows: Chapter 2 provides the formulation and derivation of the metastructure beam mathematical model coupled with the local absorbers. The obtained reduced order model and the numerical solution approach are also presented. Chapter 3 deals with the linear free and forced vibration analyses of the metastructure. The effect of adding absorbers and tuning their frequencies and damping ratios is investigated. In Chapter 4, the nonlinear frequency response of the metamaterial beam is examined. The impact of adding absorbers and modulating their frequencies on the nonlinear response of the beam is discussed. Finally, in Chapter 5, we perform an optimization analysis to maximize the vibration suppression by the appropriate selection of the local absorbers' tuning frequencies. The tuning frequencies of the absorbers are optimized to achieve the maximum possible mitigation of the beam with few absorbers.

Chapter 2. Nonlinear Metamaterial Beam Model

In this thesis, a metastructure beam is under investigation. Before getting into the formulation of the beam embedded with the absorbers, the derivation of the Mettler beam model is presented. A beam is a slender three-dimensional body with one geometric dimension prevailing over the other, and hence it is modelled as a one-dimensional structure

2.1. Mettler Model Derivation From Euler-Bernoulli Beam Model

The straight stress-free configuration is taken as the reference configuration. The fixed frame of reference is denoted by (O, e_1, e_2, e_3) as seen in Figure 2.1. A reference line C° in B° is chosen as a base curve. In the derivation of this theory, the rigidity of the cross sections according to which they are assumed to fully preserve their original shape no matter what the loading conditions are.

From Figure 2.1, let $r(s,t)$ be the position vector of C. Moreover, it is proved in [63] that the base fiber $\partial_s r^\circ$ orthogonal to the cross section at s is transformed into $v := \partial_s r$. This vector is called stretch vector and it has two projection as seen in Figure 2.2.

The stretch vector is written as:

$$\boldsymbol{v}(s,t) =: v(s,t)\boldsymbol{b_1}(s,t) + \eta(s,t)\boldsymbol{b_2}(s,t) \tag{2.1}$$

where

$$v := \partial_s \boldsymbol{r}.\boldsymbol{b_1} \;\; and \;\; \eta := \partial_s \boldsymbol{r}.\boldsymbol{b_2} \tag{2.2}$$

denote the beam stretch and the shear strain, respectively. Moreover, the rate of change of the rotation angle θ with respect to the arclength s is defined as:

$$\mu(s,t) := \partial_s \theta(s,t) \tag{2.3}$$

This is not the geometric curvature but is known as the bending curvature which is completely different. Consequently, the geometric boundary conditions are in the form:

$$\boldsymbol{r}(0,t) = \overline{\boldsymbol{r_1}}(t),\ \boldsymbol{r}(l,t) = \overline{\boldsymbol{r_2}}(t),\ \theta(0,t) = \overline{\theta_1}(t),\ \theta(l,t) = \overline{\theta_2}(t) \tag{2.4}$$

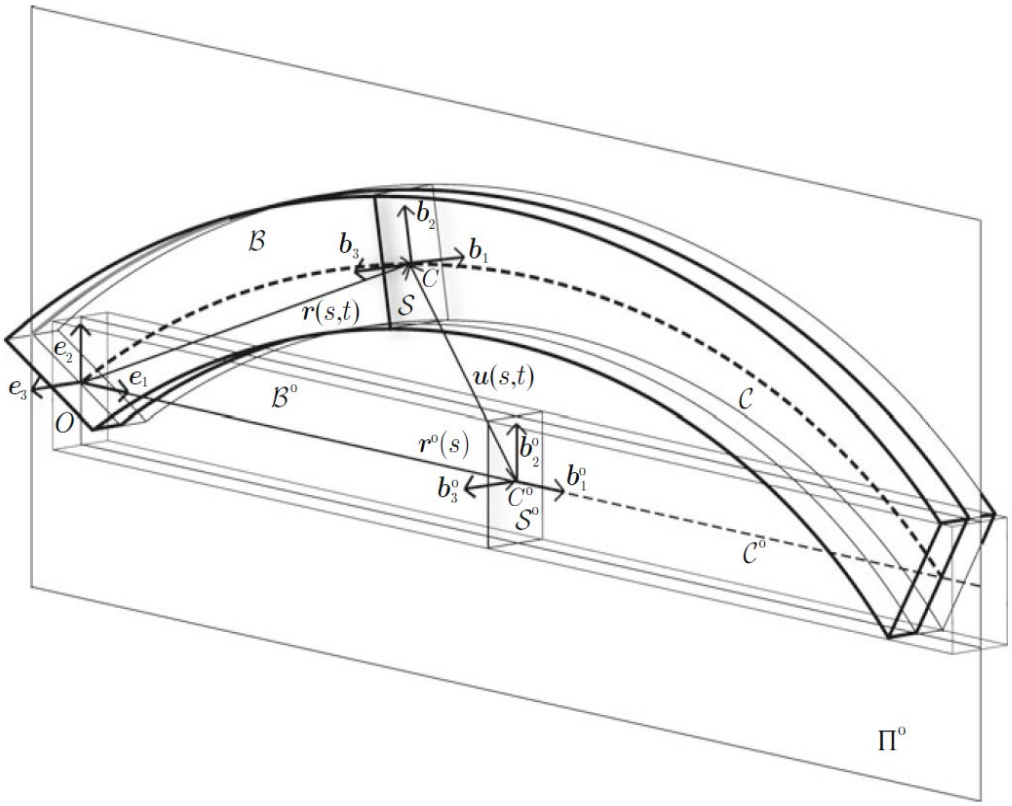

Figure 2.1: Planar motion of a beam [63]

The strains expressed in terms of the displacement gradient $u_s = u_s e_1 + v_s e_2$ become

$$v(s,t) = (1+u_s)\cos\theta + v_s \sin\theta, \quad \eta(s,t) = -(1+u_s)\sin\theta + v_S \cos\theta \quad (2.5)$$

where the subscript s means differentiation with respect to s. Moreover, using the Taylor expansion and the linearization of the strain-displacement relationships, the result gives:

$$v^{(1)} = u_s^{(1)}, \quad \eta^{(1)} = v_s^{(1)} - \theta^{(1)}, \; and \; \mu^{(1)} = \theta_s^{(1)} \quad (2.6)$$

2.1.1. Nonlinear strains in 3d theory. The position vector (an arbitrary point) of the base curve is

$$\boldsymbol{p}(s,t) = r_1\boldsymbol{e_1} + r_2\boldsymbol{e_2} + x_2\boldsymbol{b_2} + x_3\boldsymbol{b_3} =$$
$$(r_1 - x_2\sin\theta)\boldsymbol{e_1} + (r_2 + x_2\cos\theta)\,\boldsymbol{e_2} + x_3\boldsymbol{e_3} \quad (2.7)$$

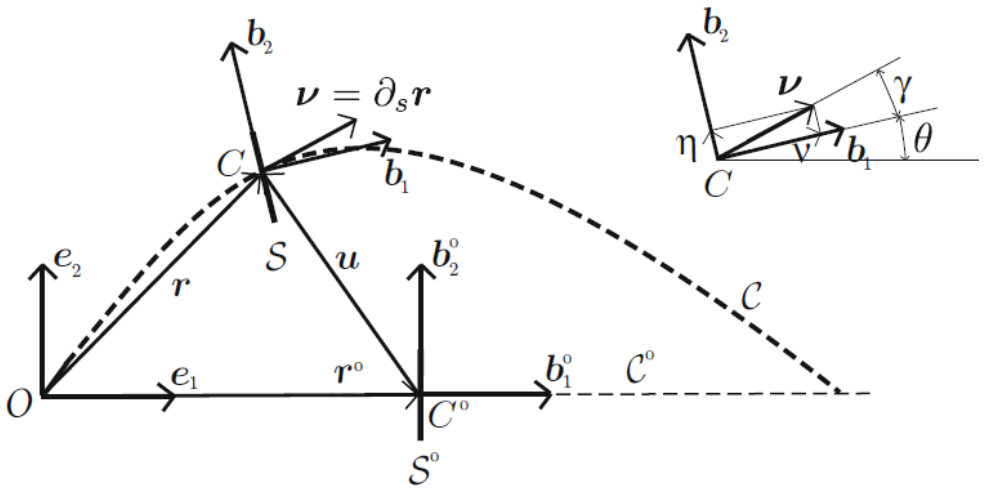

Figure 2.2 Planar motion of beam: stretch vector and strains as components of the $\mathbf{v}$ [63]

The deformation gradient can be calculated according to $\boldsymbol{F}^T = \nabla \boldsymbol{p} = \left(\boldsymbol{e_1}\partial_{x_1} + \boldsymbol{e_2}\partial_{x_2} + \boldsymbol{e_3}\partial_{x_3}\right)(p_1\boldsymbol{e_1} + p_2\boldsymbol{e_2} + p_3\boldsymbol{e_3})$, from which

$$\begin{aligned}\boldsymbol{F} = (\partial_s r_1 - x_2\partial_s\theta\cos\theta)\boldsymbol{e_1}\boldsymbol{e_1} + \cos\theta\boldsymbol{e_2}\boldsymbol{e_2} + \boldsymbol{e_3}\boldsymbol{e_3} \\ +(\partial_s r_2 - x_2\partial_s\theta\sin\theta)\boldsymbol{e_2}\boldsymbol{e_1} - \sin\theta\boldsymbol{e_1}\boldsymbol{e_2}\end{aligned} \quad (2.8)$$

with $\partial_{x_1} = \partial_s$.

By using the definition of the stretch vector [63],

$$\boldsymbol{v_1} = \boldsymbol{F}\cdot\boldsymbol{b_1} = (\partial_s r_1 - x_2\partial_s\theta\cos\theta)\,\boldsymbol{e_1} + (\partial_s r_2 - x_2\partial_s\theta\sin\theta)\boldsymbol{e_2} \quad (2.9)$$

The magnitude of v_1 is the stretch of the material fiber given by

$$v_1 = [\,(\partial_s r_1)^2 + (\partial_s r_2)^2 - 2x_2\partial_s\theta(\partial_s r_1\cos\theta + \partial_s r_2\cos\theta) + x_2^2(\partial_s\theta)^2]^{\frac{1}{2}} \quad (2.10)$$

If the material fiber coincides with the base curve, it is $x_2 = 0$, from which the stretch vector and it s magnitude, become,

$$\boldsymbol{v_1^\circ} = \partial_s r_1\boldsymbol{e_1} + \partial_s r_2\boldsymbol{e_2} \;\; and \; v_1^\circ = \sqrt{(\partial_s r_1)^2 + (\partial_s r_2)^2} = |\partial_s\boldsymbol{r}| \quad (2.11)$$

where the superscript ° refers to the a quantity in the base curve.

On the other hand, the shear strain (check the basic deformation of shear strain!) between the material fiber collinear with the baseline and the material line of the cross section collinear with $b_2^\circ = e_2$ is found to be

$$\sin\gamma^\circ = \partial_s \boldsymbol{r} \cdot \boldsymbol{b_2}/v_1^\circ = (-\sin\theta\ \partial_s r_1 + \cos\theta\ \partial_s r_2)/|\partial_s \boldsymbol{r}| \tag{2.12}$$

where γ is the shear strain between the material fibers $b_1^\circ\ and\ b_2^\circ$.

The vector $\partial_s r = \partial_s r_2 e_1 + \partial_s r_2 e_2$ is projected along the unit vectors (b_1, b_2) obtaining

$$\partial_s \boldsymbol{r}.\boldsymbol{b_1} = \partial_S r_1 \cos\theta + \partial_s r_2 \sin\theta, \quad \partial_S \boldsymbol{r} \cdot \boldsymbol{b_2} = -\partial_s r_1 \sin\theta + \partial_s r_2 \cos\theta \tag{2.13}$$

By revisiting Eq. (2.2)

$$v \coloneqq \partial_s\, \boldsymbol{r}.\boldsymbol{b_1} \ \ and\ \ \eta \coloneqq \partial_s\, \boldsymbol{r}.\boldsymbol{b_2}$$

It follows that

$$\eta = v_1^\circ \sin\gamma^\circ, \ \ v = v_1^\circ \cos\gamma^\circ = \sqrt{\left(v_1^\circ\right)^2 - \eta^2} \tag{2.14}$$

which are the beams stretch and shear strain respectively.

Moreover, the bending (flexural) curvature is given by:

$$\mu(s,t) \coloneqq \partial_s \theta(s,t) \tag{2.15}$$

Again, this is different from the geometric curvature which is given as:

$$\mu^G = \frac{\partial\phi}{\partial_s}\frac{\partial_s}{\partial_{\hat{s}}} = \frac{\partial_s\theta + \partial_s\gamma}{|\partial_s \boldsymbol{r}|} = \frac{\mu + \partial_s\gamma}{v_1^\circ} \tag{2.16}$$

To ensure the motions are admissible, the condition det F > 0 must be enforced and therefore leading to

$$det\, \boldsymbol{F} = v - x_2\mu > 0 \tag{2.17}$$

2.1.2. The Euler-Bernoulli beam. The Euler-Bernoulli assumes a beam being sufficiently slender and thus the shearing effects turn out to be barely appreciable [63]. This unshearability $(\eta = 0)$ leads to kinematic and strain-displacement relationships denoted as follows:

$$\boldsymbol{r_s} = v\boldsymbol{b_1},\ \cos\theta = \frac{1+u_s}{v},\ \sin\theta = \frac{v_s}{v},\quad \theta = \arctan\left(\frac{v_s}{1+u_s}\right) \tag{2.18}$$

$$v = \sqrt{(1+u_s)^2 + v_s^2},\qquad \mu = [v_{ss}(1+u_s) - u_{ss}v_s]/v^2 \tag{2.19}$$

Solving the inextensibility constraint with respect to the horizontal displacement gradient u_s and v given as above, and substituting the result into the bending curvature above, one gets

$$u_s = -1 \pm \sqrt{1-v_s^2},\ \theta = \pm\arctan\left(\frac{v_S}{\sqrt{1-v_s^2}}\right),\ \mu = \pm\frac{v_{ss}}{\sqrt{1-v_s^2}} \tag{2.20}$$

Only the plus sign is meaningful. The obtained kinematic relationships show that the problem can be formulated in terms of one kinematic unknown only, namely, the transverse displacement $v(s,t)$. The obtained beam model is referred to as the Euler-Bernoulli beam model. The linearization of the kinematic relationships of the Euler-Bernoulli beams yields:

$$\theta^{(1)} = v_s^{(1)} \quad and\ \mu^{(1)} = v_{ss}^{(1)} \tag{2.21}$$

2.1.3. Equations of motion. The equations of motion will be derived. First, we introduce the linear and angular momentum per unit reference length:

$$\boldsymbol{l}(s,t) \coloneqq \int_S \partial_t \boldsymbol{p}(s,t)\rho(s)dA,\ \ \boldsymbol{h}(s,t) \coloneqq \int_S \boldsymbol{p}(s,t) \times \partial_t \boldsymbol{p}(s,t)\rho(s)dA \tag{2.22}$$

where $\partial_t\, \boldsymbol{p}(s,t)$ is the velocity of the material points (recall the $p = r(s,t) + x_2 b_2 + x_3 b_3$) of the cross section at s which occupy the current position $\boldsymbol{p}(s,t)$. The derivative of the position vector given above can be written as $\partial_t \boldsymbol{p}(s,t) = \partial_t \boldsymbol{r}(s,t) + x_2 \partial_t \boldsymbol{b_2}(s,t)$. This allows us to write the linear and angular momentum per unit reference length as:

$$\boldsymbol{l}(s,t) = \int_S [\partial_t \boldsymbol{r} + x_2 \partial_t \boldsymbol{b_2}]\rho(s)dA = \rho A(s)\partial_t \boldsymbol{r} + \rho I(s)\partial_t \boldsymbol{b_2} \tag{2.23}$$

$$\begin{aligned} h(s,t) &= \int_S [\boldsymbol{r} + (x_2\boldsymbol{b_2} + x_3\boldsymbol{b_3})] \times [\partial_t \boldsymbol{r} + x_2 \partial_t \boldsymbol{b_2}]\rho(s)dA \\ &= \boldsymbol{r} \times [\rho A(s)\partial_t \boldsymbol{r} + \rho I(s)\partial_t \boldsymbol{b_2}] + \boldsymbol{b_2} \times [\rho I(s)\partial_t \boldsymbol{r} + \rho J(s)\partial_t \boldsymbol{b_2}] \end{aligned} \tag{2.24}$$

where

$$\rho A(s) \coloneqq \int_S \rho(s)dA\,, \rho I(s) \coloneqq \int_S x_2\rho(s)dA\,,\ \rho J(s) \coloneqq \int_S x_2^2\rho(s)dA \qquad (2.25)$$

The beam mass per unit length is $\rho A(s)$. The first and second mass moments of area with respect to the axis collinear with $\boldsymbol{b_3}$ are $\rho I(s)\ and\ \rho J(s)$.

Let $\boldsymbol{n}(s,t) \coloneqq N(s,t)\,\boldsymbol{b_1}(s,t) + Q(s,t)\,\boldsymbol{b_2}(s,t)\ and\ \boldsymbol{m}(s,t) = M(s,t)\ \boldsymbol{e_3}$ denote the beam generalized stress resultants and contact couple (bending moment). N is the tension, Q is the shear force, M is the bending moment.

The balance of linear and angular momentum of the beam is enforced through

$$\boldsymbol{f_1} + \boldsymbol{f_2} + \int_0^l \boldsymbol{f}\,ds = \frac{d}{dt}\int_0^l \boldsymbol{l}\,ds,$$
$$c_1 + c_2 + \int_0^l \boldsymbol{r}\times\boldsymbol{f}\,ds + \int_0^l \boldsymbol{c}\,ds + \boldsymbol{r}(l,t)\times\boldsymbol{f_2} = \tfrac{d}{dt}\int_0^l \boldsymbol{h}\,ds \qquad (2.26)$$

where $\boldsymbol{f}$ and $\boldsymbol{c}$ are the resultant applied force and resultant couple per unit length. Moreover, $(\boldsymbol{f_1}, \boldsymbol{c_1})$ and $(\boldsymbol{f_2}, \boldsymbol{c_2})$ are the resultant forces and couples at the beam ends $s = 0$ and $s = l$, respectively.

The balance of linear and angular momentum is enforced on the beam part according to

$$-\boldsymbol{n}(s_1,t) + \int_{s_1}^{s} \boldsymbol{f}(\xi,t)d\xi = \tfrac{d}{dt}\int_{s_1}^{s} \boldsymbol{l}(\xi,t)d\xi - \boldsymbol{r}(s_1,t)\times\boldsymbol{n}(s_1,t) + \boldsymbol{r}(s,t)\times\boldsymbol{n}(s,t) -$$
$$\boldsymbol{m}(s_1,t) + \boldsymbol{m}(s,t) + \int_{s_1}^{s} \boldsymbol{c}d\xi + \int_{s_1}^{s} \boldsymbol{r}\times\boldsymbol{f}\,d\xi = \tfrac{d}{dt}\int_{s_1}^{s} \boldsymbol{h}(\xi,t)d\xi \qquad (2.27)$$

By applying the integration-by-part rules, we gain one vector-valued equation and one scalar equations as follows:

$$\partial_s\boldsymbol{n} + \boldsymbol{f} = \rho A\partial_{tt}\boldsymbol{r} + \rho I\partial_{tt}\boldsymbol{b_2} \qquad (2.28)$$
$$\partial_s\boldsymbol{M} + (\boldsymbol{v}\times\boldsymbol{n})\cdot\boldsymbol{e_3} + c = \{\boldsymbol{b_2}\times[\rho I\partial_{tt}\boldsymbol{r} + \rho J\partial_{tt}\boldsymbol{b_2}]\}\cdot\boldsymbol{e_3} \qquad (2.29)$$

where $v \coloneqq \partial_s r$ is the stretch vector of the base curve at s and time t. Hence, if the base curve C° is taken to be the beam centerline, the equations of motion reduce to the simpler form:

$$\partial_s\boldsymbol{n} + \boldsymbol{f} = \rho A\partial_{tt}\boldsymbol{r}, \qquad (2.30)$$
$$\partial_s\boldsymbol{M} + (\boldsymbol{v}\times\boldsymbol{n})\cdot\boldsymbol{e_3} + c = \rho I\partial_{tt}\theta \qquad (2.31)$$

2.1.4. Simplification of the angular momentum. After relaxing the assumption that the section-fixed director b_2 was always assumed to be collinear to the axis of symmetry of the beam, and rewriting Eq. (2.24). we get the following expression of the angular momentum

$$\begin{aligned}\boldsymbol{h}(s,t) = \int_S [\boldsymbol{r} + (x_2\boldsymbol{b_2} + x_3\boldsymbol{b_3})] \times [\partial_t \boldsymbol{r} + x_2\partial_t \boldsymbol{b_2}]\rho(s)dA \\ = \boldsymbol{r} \times (\rho A \partial_t \boldsymbol{r} + \rho I_3 \partial_t \boldsymbol{b_2}) \\ + \boldsymbol{b_2} \times (\rho I_3 \partial_t \boldsymbol{r} + \rho J_{33} \partial_t \boldsymbol{b_2}) + \boldsymbol{b_3} \times (\rho I_2 \partial_t \boldsymbol{r} - \rho J_{23} \partial_t \boldsymbol{b_2}) \end{aligned} \quad (2.32)$$

where

$$\rho I_2 := \int_S x_3 \rho dA, \;\; \rho I_3 = \rho I := \int_S x_2 \rho dA,$$

$$\rho J_{33} = \rho J := \int_S x_2^2 \rho dA, \;\; \rho J_{23} = \rho J := -\int_S x_2 x_3 \rho dA$$

Here, $\rho J_{ij} b_i b_j$ is the inertia tensor of the cross section. If b_2 is collinear to the axis of symmetry, then

$$\rho I_2 := \int_S x_3 \rho dA = 0\,, \;\; \rho J_{23} := -\int_S x_2 x_3 \rho dA = 0$$

2.1.5. Component form of the equations of motion. Let $\boldsymbol{r} := \boldsymbol{r}^{\circ} + u_1\boldsymbol{b_1} + u_2\boldsymbol{b_2}$so that the acceleration in the local basis can be obtained. The ensuing component form of the equations of motion is

$$\partial_s N - \mu Q + f_1^b = \rho A[\partial_{tt} u_1 - (\partial_t \theta)^2 u_1 - 2\partial_t u_2 \partial_t \theta - u_2 \partial_{tt} \theta] \quad (2.33)$$

$$\partial_s Q + \mu N + f_2^b = \rho A[\partial_{tt} u_2 - (\partial_t \theta)^2 u_2 + 2\partial_t u_1 \partial_t \theta - u_1 \partial_{tt} \theta] \quad (2.34)$$

$$\partial_s M + vQ - \eta N + c = \rho I \partial_{tt} \theta \quad (2.35)$$

where $f_k^b := \boldsymbol{f} \cdot \boldsymbol{b_k}, \;\; k = 1,2$

When we consider the case of unshearable beams, when the material constraint $\eta = 0$ is introduced into Eq. (2.33), the reactive shear force Q yields,

$$Q = -(\partial_s M + c - \rho J \partial_{tt} \theta)/\, v \quad (2.36)$$

The shear force is then substituted into Eq. (2.31) and becomes the equations of contrained motion for unshearable beams

$$\rho A[\partial_{tt}u_1 - (\partial_t\theta)^2 u_1 - 2\partial_t u_2 \partial_t\theta - \partial_{tt}\theta u_2] + \frac{\mu}{v\rho I\partial_{tt}\theta}$$
$$-\partial_s N - \left(\frac{\mu}{v}\right)\partial_s M = f_1^b + \left(\frac{\mu}{v}\right)c \tag{2.37}$$

2.1.6. Axially restrained elastic beams. An explicit expression of the tension can be found once the constitutive equation for a linearly elastic beam is expressed in the form $N(s,t) = EA\epsilon(s,t)$. The uniformity of N allows its computation as an average of the domain $[0, l]$:

$$\widehat{N}(t) = \frac{1}{l}\int_0^l \widehat{N}ds = \frac{1}{l}\int_0^l EA\left(u_s + \frac{1}{2}v_s^2\right)ds$$
$$= \frac{EA}{l}[u(l,t) - u(0,t)] + \frac{EA}{l}\int_0^l \frac{1}{2}v_s^2 ds \tag{2.38}$$

The next step is to consider the equation of motion in the transverse direction by introducing the following approximations:

$$\widehat{\boldsymbol{M}}(s,t) = EIv_{ss}, \quad \left(\frac{M_s}{v}\right)_s \sim M_{ss} = (EIv_{ss})_{ss},$$

$$\boldsymbol{f}\cdot\boldsymbol{b_2} \sim \boldsymbol{f}\cdot\boldsymbol{e_2} = f_2, \qquad \rho A\boldsymbol{r_{tt}}\cdot\boldsymbol{b_2} \sim \rho A v_{tt}, \qquad and\ \ \mu N \sim v_{ss}\widehat{N}$$

The resulting approximate equation of motion is the following integral-partial-differential equation which was first proposed by Mettler

$$\rho A v_{tt} + EIv_{ssss} - \frac{EA}{l}v_{ss}[u(l,t) - u(0,t)] - \frac{EA}{2l}v_{ss}\int_0^l v_s^2 ds = f_2 \tag{2.39}$$

Eq. (2.37) was first proposed by Mettler [23] and is employed in our study of nonlinear structural dynamics. This equation, however, has a limited range of validity, mostly restricted to linearly elastic beams that are: (a) axially restrained at the boundaries, (b) not loaded by resonant longitudinal forces, and (c) loaded by moderate transverse forces f_2 so that the resulting flexural motions are of moderately large amplitude in agreement with hypotheses (b) and (c) and with the second-order kinematic truncation of the elongation.

2.2. Metastructure Mathematical Model

The metamaterial beam modeled as a Mettler beam as in Eq. (2.37) is coupled with an array of N_{va} linear vibrator absorber each having mass m_i. By investigating Figure 2.3, the effect of the local resonators will be considered as an external force (point forces) at particular spatial locations along the beam. Moreover, the displacement of the i^{th} mass relative to the cross section centerline is represented by $\overline{y_i}(t)$. Thus the Euler-Bernoulli equation becomes

$$\rho A\ddot{v} + c_2\dot{v} + EI\partial_{ssss}v - \frac{EA}{l}\partial_{ss}v\int_0^l \frac{1}{2}\partial_s v^2 ds + \sum_{i=1}^{N_{va}} m_i[\ddot{v}(s_i,t) + \ddot{\overline{y}}_i(t)]\delta(s-s_i) = f_2(s,t) \tag{2.40}$$

where $\delta(s-s_i)$ is the Dirac delta function representing the concentrated force exerted by the ith absorber. The equation of motion of a typical absorber is given as

$$m_i[\ddot{v}(s_i,t) + \ddot{\overline{y}}_i(t)] + c_i\dot{\overline{y}}_i(t) + k_i\overline{y}_i(t) = 0 \tag{2.41}$$

2.2.1. Nondimensionalization. The equations of motion are rendered nondimensional by rescaling time by the characteristic time $\frac{1}{\omega_c} = \sqrt{\frac{\rho Al^4}{EI}}$ and the displacement by the beam span l. Therefore, $s^* = \frac{s}{l}$, $t^* = \omega_c t$, $v^* = \frac{v}{l}$ and $y_i = \overline{y_i}/l$. The equations of motion in nondimensional form become

$$\ddot{v} + 2\zeta\dot{v} + v'''' - \lambda^2 v''\int_0^l \frac{1}{2}(v')^2 ds + \sum_{i=1}^{N_{va}} \mu_i\left[\ddot{v}_{s_i} + \ddot{y}_i\right]\delta(s-s_i) = f_2,$$

$$\mu_i\left[\ddot{v}_{s_i} + \ddot{y}_i\right] + 2\zeta_i\mu_i\alpha_i\bar{\omega}\dot{y}_i + \mu_i\alpha_i^2\bar{\omega}^2 y_i + N_i(y_i^2, y_i^3) = 0 \tag{2.42}$$

where the stars are dropped and the following nondimensional parameters were introduced

$$\zeta = \frac{c_2}{2\rho A\omega_c}, \qquad \lambda^2 = \frac{EAl^2}{EI}, \qquad \bar{\omega} = \frac{\omega_{cr}}{\omega_c}$$

$$\mu_i = \frac{m_i}{\rho Al}, \qquad \alpha_i = \frac{\omega_{va}}{\omega_{cr}}, \qquad \zeta_i = \frac{c_i}{2m_i\omega_{va_i}}, \qquad \omega_{va}^2 = \frac{k_i}{m_i} \tag{2.43}$$

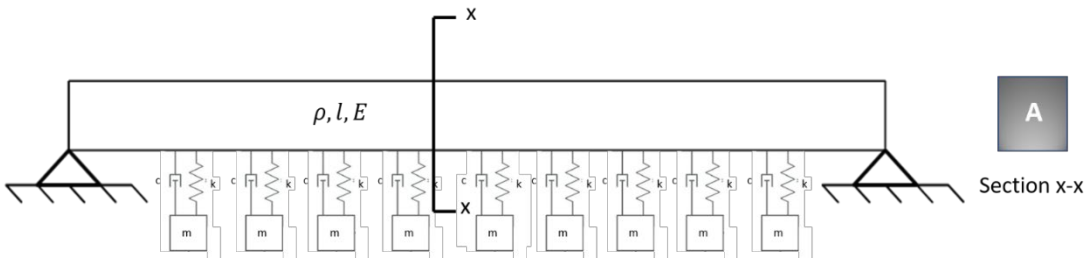

Figure 2.3 Schematic of the metamaterial hinged-hinged beam

The mass ratio and linear frequency of the i^{th} absorber are denoted by $\mu_i$and $\omega_{va,i}$. Moreover, α_i represents the ratio of the absorber frequency to the frequency to be controlled, $\bar{\omega}$ is the ratio of frequency to be controlled to the characteristic frequency, ζ_i is the linear damping frequency factor of the i^{th} absorber.

2.2.2. Galerkin discretization. Next, the Galerkin's discretization method is used to reduce the dependence of the equations of motion on the space and end up with a finite set of ordinary differential equations in time only By referring back to Rao [62], the mode shapes of a hinged-hinged beam can be seen in Figure 2.4.

$$v(s,t) = \sum_{k=1}^{N_m} q_k(t)\phi_k(s) \tag{2.44}$$

where N_m is the number of modes retained in the discretization, $q_k(t)$ is the kth generalized coordinate, and $\phi_k(s)$ is the corresponding trial function taken as the kth eigenfunction normalized according to $\int_0^1 \phi_k^2(s)ds = 1$.

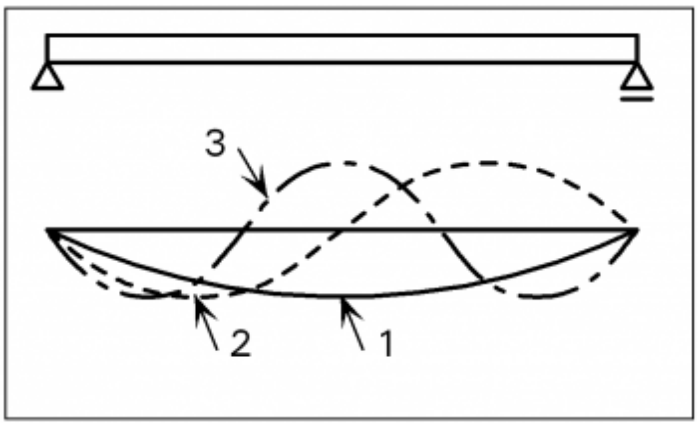

Figure 2.4 The lowest mode shapes of the hinged-hinged beam [63]

The trial function for the simple supported beams is

$$\phi_k(s) = \sqrt{2}\sin\left(\frac{k\pi s}{l}\right) \tag{2.45}$$

Substituting Eq. 2.42 into the equation of motion in the non-dimensional form Eq. (2.40), the kth Galerkin-reduced equation is

$$\begin{aligned}\int_0^1 \phi_k\{\sum_{j=1}^{N_m}[\ddot{q}_j\phi_j + 2\zeta\dot{q}_j\phi_j + q_j\phi_j'''' \\ -\lambda^2 q_j\phi_j''\int_0^1 \frac{1}{2}\left(q_j\phi_j\right)^2 ds - f_2(s,t) \\ + \sum_{i=1}^{N_m}\mu_i\left[\sum_{j=1}^{N_m}\ddot{q}_j\phi_j(s_i) + \ddot{y}_i\right]\delta(s-s_i)\}\, ds = 0\end{aligned} \tag{2.46}$$

while the equation of motion of the ith absorber becomes

$$\mu_i\left[\sum_{j=1}^{N_m}\ddot{q}_j\phi_j(s_i) + \ddot{\bar{y}}_i\right] + 2\zeta_i\mu_i\alpha_i\bar{\omega}\dot{y}_i + \mu_i\alpha_i^2\bar{\omega}^2 y_i + N(y_i^2, y_i^3) = 0 \tag{2.47}$$

The orthogonality conditions of modes, are used to simplify the discretized equations. The equations of motion is projected onto the modal space and is expressed in matrix form. By introducing $x = \{q_k, y_i\}$, we obtain,

$$\boldsymbol{M}\ddot{\boldsymbol{x}} + \boldsymbol{C}\dot{\boldsymbol{x}} + \boldsymbol{K}\boldsymbol{x} + \boldsymbol{N} - \boldsymbol{f} = 0 \tag{2.48}$$

where $\boldsymbol{M}, \boldsymbol{C}$ and $\boldsymbol{K}$ are the mass, damping and stiffness matrices, respectively, in the modal space; f is the vector containing the modal components of the external excitations, and N is the vector containing the quadratic and cubic nonlinearities expressed in modal coordinates.

The obtained ODE can be further expressed in state space by introducing $y = \dot{x}$ and $z = \{x, y\}$. The dynamic system in its compact form can be written as

$$\dot{\boldsymbol{z}} = \boldsymbol{A}\boldsymbol{z} - \widetilde{\boldsymbol{N}} + \tilde{\boldsymbol{f}} \tag{2.49}$$

where

$$\boldsymbol{A} = \begin{bmatrix} \boldsymbol{0} & \boldsymbol{I} \\ -\boldsymbol{M}^{-1}\boldsymbol{K} & -\boldsymbol{M}^{-1}\boldsymbol{C} \end{bmatrix},\ \widetilde{\boldsymbol{N}} = \begin{bmatrix} \boldsymbol{0} \\ -\boldsymbol{M}^{-1}\boldsymbol{N} \end{bmatrix},\ \tilde{\boldsymbol{f}} = \begin{bmatrix} \boldsymbol{0} \\ -\boldsymbol{M}^{-1}\boldsymbol{f} \end{bmatrix}$$

Equations (2.46) and (2.47) will be further demonstrated and explained in the upcoming chapters. Essentially, the equations of motion should be written in the Matrix format to keep it programming friendly. This means that the equations are in a format to be solved using Matlab.

After going through the derivation of the beam model, the equation is tweaked to include the effect of the local absorbers and any external forces. The non-dimensionalization technique is then implemented to simplify and parametrize the problem. The resulting equation was an integro-differential equation. It is, in fact, hard to solve. Therefore, the mode shapes of a hinged-hinged beam is utilized and the Galerkin discretization is implemented. The equation becomes a set of ordinary differential equations and the orthogonality conditions eases the computation. Furthermore, the equations are written in a matrix format to include it in a software package such as Matlab and do the investigations.

With the equations in hand, the first step is to analyze the beam in the linear regime. This means the entries of N is Eq. (2.46) is disregarded. The analysis is shown next.

Chapter 3. Linear Free and Forced Vibration Analysis

In this chapter, we conduct a linear analysis to gain an insight on the dynamic behavior of the metamaterial beam when ignoring the geometric nonlinearity. In the subsequent analysis, we consider a beam having an undeformed length $l = 1\ m$, a cross sectional area $A = 0.00103\ \mathrm{m}^2$ and an inertia moment $I = 1.71 \times 10^{-6}\ m^4$. The metamaterial is made of a homogenous elastic material with a mass density $\rho = 7860\ kg/m^3$ and a Young's modulus $E = 210\ GPa$. The damping ratio is set to $\zeta = 1\%$. The parameters are summarized in Table 3.1 at the end of this section. Such parameter lead to a value of characteristic frequency of $\omega_c = 210\ Hz$. Moreover, the first six natural frequencies of the beam under study are given in Table 3.2.

Table 3.1: Parameters of the metastructure beam

Parameter	**Magnitude**
Length (l)	1 m
Area (A)	$0.00103\ m^2$
Moment of intertia (I)	$1.71 \times 10^{-6}\ m^4$
Density (ρ)	$7860\ kg/m^3$
Young's modulus (E)	$210\ GPa$
Damping Ratio (ζ)	1%
Characteristic frequency (ω_c)	210 Hz

Table 3.2: The natural frequencies of the first six bending modes

Mode	**Frequency [Hz]**
First	330.825
Second	1323.298
Third	2977.42
Fourth	5293.19
Fifth	8270.6
Sixth	11909.68

In this section, the behavior of the finite host (beam) embedded with an array of resonators is investigated. The transfer matrix method is implemented to achieve the linear dynamic response of the metamaterial beam.

The ordinary differential equations, Eqs. (2.46), are further expressed in state-space form by introducing the vector collecting the velocities of the variables $y = \dot{x} = \{p_k, y_{p,i}\}$. The augmented dynamics system becomes

$$\begin{aligned} \dot{x} &= y \\ M\dot{y} + Cy + Kx + N - f &= 0 \end{aligned} \tag{3.1}$$

The forcing term f is assumed to be harmonic in the form $f = Fe^{i\Omega t}$. From the first part of Eq. (3.1), since the differential equation is homogenous, one can express the following:

$$x = Xe^{i\Omega t} \tag{3.2}$$

Moreover, since *y* is the first derivative of *x*, one can express the following:

$$y = \dot{x} = i\Omega Xe^{i\Omega t} \tag{3.3}$$

By assuming the forcing term to be harmonic and substituting the assumed harmonic solution into Eq. (3.1), we obtain

$$[-\Omega^2 M + i\Omega C + K]\, X = F \tag{3.4}$$

This equation is written in a matrix format to ease up the computation and be able to program it. As a reminder, x is the vector of generalized coordinates $x = \{q_k, y_i\}$ whose size is $[(N_{modes} + N_{absorbers}) \times 1]$. This means that getting the solution of x simply gives us the solution of each generalized coordinate and thus the entire response of the beam and the host structure.

By inverting the matrix in this equation, which is called the impedance matrix $H := -\Omega^2 M + i\Omega C + K$, the frequency response of the system can be obtained. Thereby, the response to the harmonic external excitation $Fe^{i\Omega t}$ can be written as

$$x = H^{-1} Fe^{i\Omega t} \tag{3.5}$$

This is the backbone expression of the linear analysis. This is a direct application where an integro-differential model (Euler-Bernoulli) was simplified into a series of

differential equations and eventually obtain a simple relation to get the solution of our generalized coordinates.

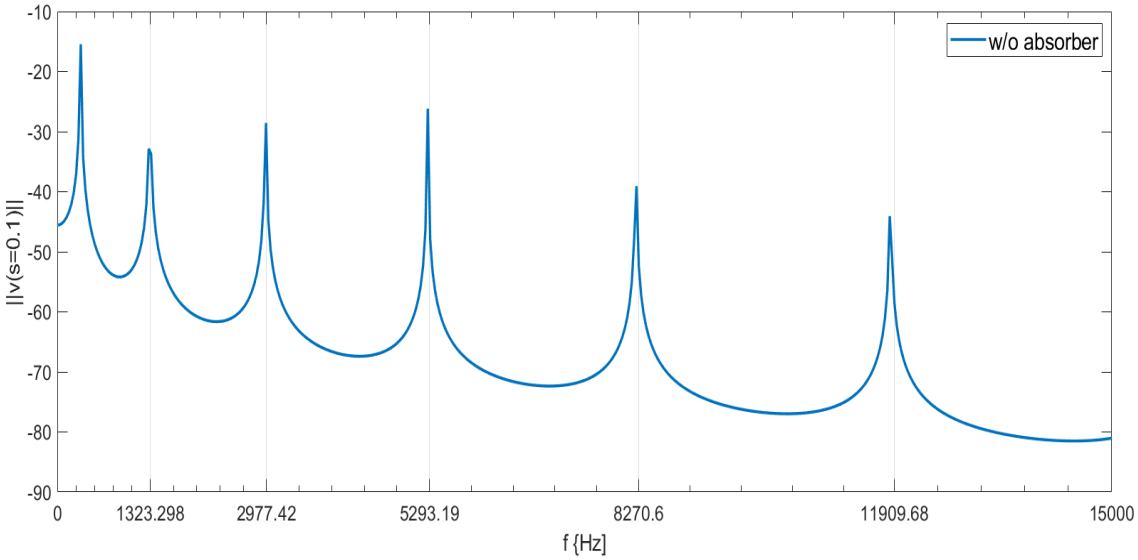

Figure 3.1: Frequency-response function of beam without absorbers

3.1. Effect of the absorbers

Initially, the aim is to verify the applicability of this equation. The frequency response of the host alone was plotted, and the forcing terms were kept as unity. The number of modes was kept as ten (10). The results are shown in Figure 3.1. The logarithmic scale is used in the y-axis and this is commonly used for frequency-response plots. This enables us to include a wide range of values.

Here, in Figure 3.1, one can notice the rise of six (6) peaks. The number of peaks are expected to be high since the number of modes implemented is 10. In fact, the frequency response depicts the natural frequency of the system. A simple code was implemented to check the first ten natural frequencies of the system and the results are shown in Table 3.1. The results in the table that are up to a frequency of 15 kHz, the fundamental six natural frequencies are present.

Therefore, Figure 3.1 showed the first six peaks which are essentially the first six modes of the structure. Our aim, as usual, is to suppress the vibration at resonant frequencies using the local absorbers. Hence, the next step is to include the effect of local absorbers.

Figure 3.2 combines the results of four different scenarios. Again, the frequency-response is plotted for a few cases. The first scenario (blue) is the same as Figure 3.1. This is the response of the host beam without absorbers. It is essential to include it as a baseline of the figure to visualize the effect of including absorbers. The subsequent cases are all showing the effect of including the absorbers. The number of absorbers was changed $N_{absorbers} = 10, 50, 100$ as well as their spatial collocation since the absorbers are evenly space and distributed along the beam. In all these cases, the absorbers were tuned to the 5^{th} mode with a frequency $f_5 = 8.27\ \ kHz$.

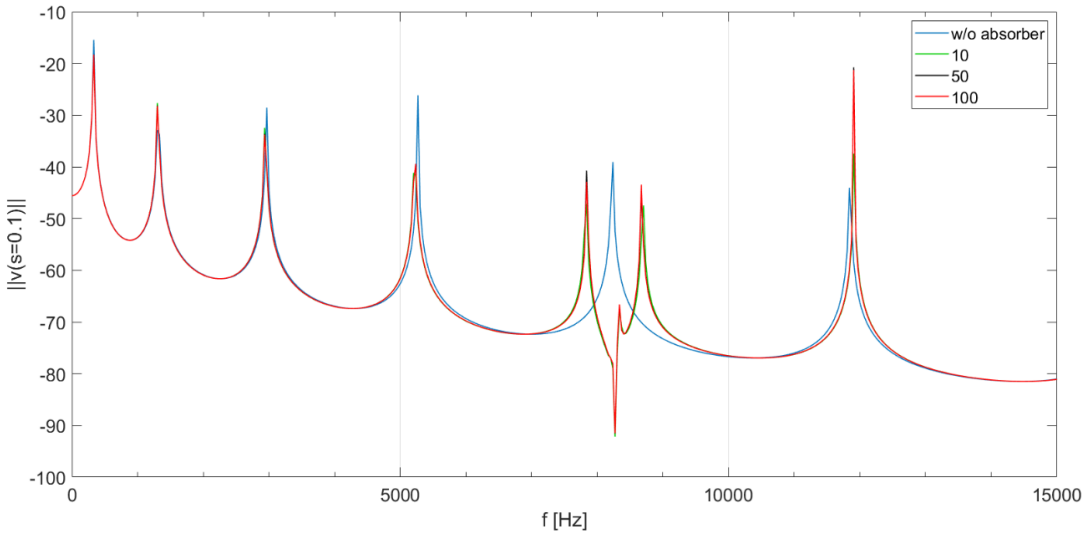

Figure 3.2: Frequency-response function of the metamaterial beam: effect of the number of absorbers.

Figure 3.2 shows the arise of the double peak phenomena. In the proximity of the fifth mode, the effect of the absorbers is very noticeable. The peak exactly at the 5^{th} natural frequency is greatly suppressed, and the peak is divided into two smaller peaks on the sides of this natural frequency. This is the effect one can depict from the addition of absorbers in general. By analyzing the number of absorbers further, one can see the effect of adding more absorbers. The amplitude of the secondary (double) peaks is still relatively high when 10 absorbers was used. The response is better than the host without absorbers, but further suppression of these peaks is needed. Therefore, the effect of integrating 50 (black) and 100 (red) absorbers is shown. The amplitude of the secondary peaks is further mitigated. The integration of absorbers proves to be beneficial. This is important in practical applications since the useful operation range

of absorbers is widened and the structure is no longer prone to face resonant effects within specific frequency ranges.

3.2. Effect of the Damping Ratio

As shown in the previous discussion, the effect of the absorbers was found to be major in suppressing the vibration of the host material when tuned at the natural frequencies of the beam. Nevertheless, this gave rise to the frequency split given the two peaks observed in the frequency response. This is simply because the new metastructure (beam + absorbers) now has a new combined natural frequency.

This double peak formed needs to be suppressed as well. Therefore, the effect of the linear damping factor of each absorber is investigated. The damping in the previous section was set to 1/1000. Here, this factor is altered and the effect is shown in Figure 3.3. The figure shows the response of hundred (100) absorbers but with different damping ratios. The figure starts to the established backbone result (without absorbers) and damping ratio set to 1/1000 shown (blue). The damping ratio is gradually increased.

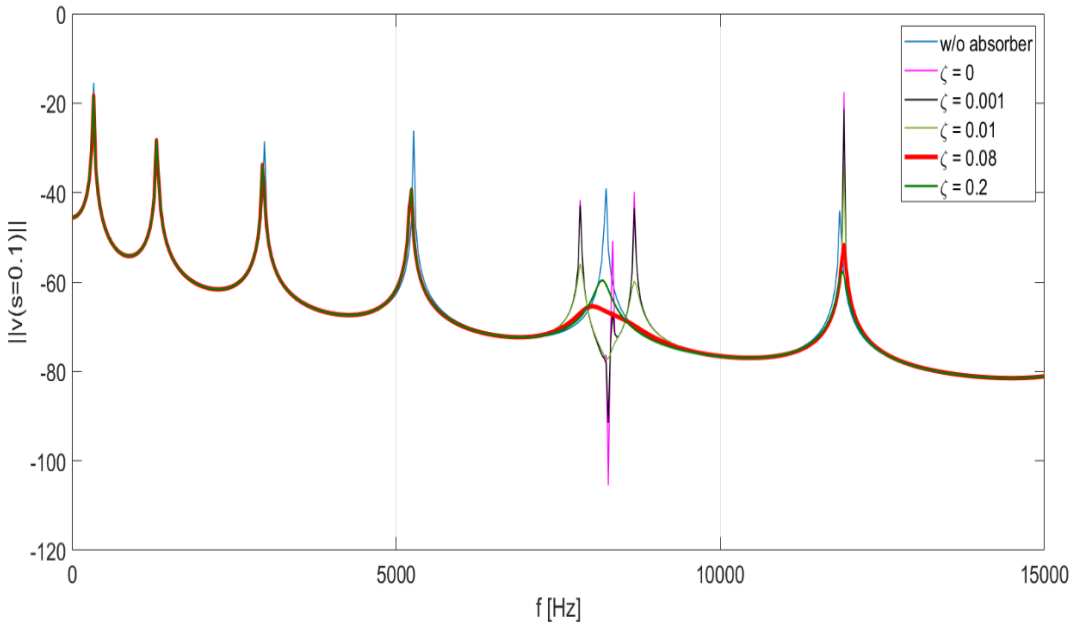

Figure 3.3: Frequency-response function of the metamaterial beam: effect of the damping ratio.

Here, Figure 3.3 shows that as the damping ratio increases, the bandwidth of operation is improved. Examination of Figure 3.3 shows that as ζ is increased, the amplification of the host structure can be reduced. Moreover, increasing ζ results in the mitigation of this double peak. The damping ratio increase shows great effects until ζ reaches around 0.08. This is the optimal damping ratio upon which the unwanted internal modes (double peaks) are almost flat (red), while the frequency stop-band is still well positioned. It is important to notice that just increasing the damping ratio does not necessarily yield the lowest amplitude. Note from Figure 3.3 that $\zeta = 0.08$ (red) produces a smaller amplification over a larger region than does the higher ratio, $\zeta = 0.2$ (green).

This means that an overestimated damping is not always a trivial solution. In fact, ζ should be varied wisely to reach an optimal value where the onset of the double peak phenomena is observed. Therefore, the optimal ζ for the given parameters is obtained using the model. This is an intriguing result since the double peak (side effect) was almost eliminated.

One needs to recall that the analysis has been done on the 5^{th} natural frequency which is almost not achievable in most practical application since the operational frequency is very large (8.27 kHz). Therefore, the linear analysis will end with a more interesting manner by operating within the first three vibration modes.

3.3. Mitigating Multiple Modes Simultaneously

The conducted linear analysis allows to study the impact of embedding absorbers to the host structure and the corresponding stop-bands over a wide frequency range. The study has been implemented on the 5^{th} mode which is in the range of 8.27 kHz. Nevertheless, the goal is to study the metastructure beam with enhanced structural damping properties, i.e limit the oscillations of the beam in a more practical range. In reality, the wide range of frequencies is of less interest. The operating range of frequencies is usually not high. This is because in structural application only the lower frequencies and thus the first few modes of the structure are of real interest, since they involve the majority of the beam mass.

Mathematically, if we go back to Eq. (2.44) which is rewritten here

$$v(s,t) = \sum_{k=1}^{N_{modes}} q_k(t)\phi_k(s)$$

The $\phi_k(s)$ is the mode shape and $q_k(t)$ is the k^{th} generalized coordinate. In simple terms, however, $q_k(t)$ can be regarded as a weighting contribution. This means that for the first mode, $q_1(t)$ ideally should have a much higher percentage than the $q_2(t)$ which is the coefficient of the second mode $\phi_2(s)$. This is because of the contribution of higher mode shapes dominance degrades as we progress. The first mode shape is the most dominant of the all, then comes the second mode and third mode and so on. The more we progress, the less significant the mode shape become since the beam barely reaches such modes.

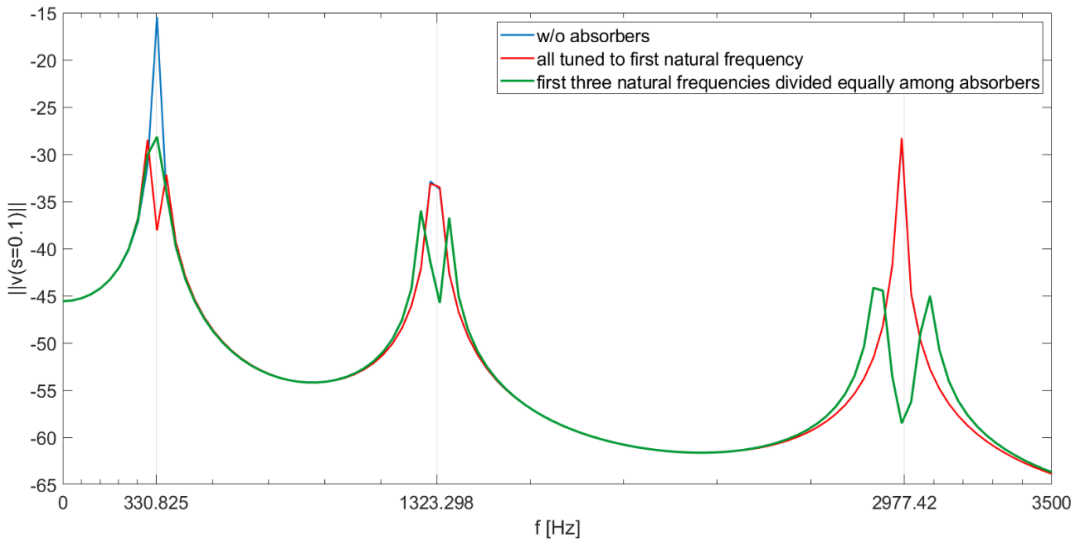

Figure 3.4: The frequency-response up to the lowest three modes. The absorbers are tuned to control the fundamental mode only (red) and the lowest three modes (green).

In light of the preceding discussion, the last result presented here in the linear regime is the analysis of the frequency response function for absorbers which were tuned to the first three modes since they are the most dominant modes. Figure 3.4 shows a combination of cases as well. The first case (blue), as usual, is the host beam with no absorbers, which is the baseline for comparison. The peaks match the first three modes as mentioned in Table 3.1. The second scenario is tuning all the absorbers (100 in this case) to the first mode. As expected, the amplification was suppressed in the proximity

of the first mode while the other two modes remain unaffected. More intriguing, the last plot (green) shows a very desirable effect. The absorbers (100) were now tuned to three different frequencies, namely to the first three modes. The first three modes are now mitigated all at once just by using different tuning frequencies for the local absorbers. This is an interesting result because using this strategy the first three modes can be suppressed simultaneously. In fact, unable to hit more than one frequency was one of the limitations of the passive vibration control over the active vibration control (i.e. using electrical components). This is an interesting outcome because by adding just 1% of the beam mass to the absorbers, the amplification near the most crucial resonant frequencies (first three modes) are decreased by tuning the parameters and hence the frequency of each absorber. Before getting into the nonlinear regimes, another interesting figure (comparison) is presented in regards of the extra mass added to the host.

3.4. Effect of Adding Extra Mass to the Host

What has been implemented in the previous analysis was integrating absorbers to the host mass to suppress the vibration at certain frequencies. The results showed promising effects. Nevertheless, absorbers, are after all, added masses. Adding extra mass to the host can simply be a suggested solution in mitigating the host vibrations. One can be skeptical that the results obtained in the previous sections might have been dominantly due to the extra mass of the absorbers rather than the tuning effect of the metastructure absorbers as suggested. Therefore, a couple of plots are shown in Figure 3.5 to justify the role of metastructure.

In Figure 3.5, the frequency response of the host with a particular mass (M) without absorbers is plotted (blue). Another frequency response is plotted over (green). However, this time the mass of the host is increased to 1.01 of the original mass, i.e. (1.01 M) is shown. The graphs are almost identical. If we just zoom in a little bit, there is a slight change in the position of the peaks due to the new mass. However, the amplitude of the peak is barely changed.

On the other hand, the third plot (red) shows frequency-response of a host structure with mass M embedded with 100 absorbers with a total absorber mass of 1%. This makes the entire structure weighs 1.01 M. Moreover, these absorbers are tuned to the 5^{th} mode. The suppression of the vibration is clearly seen. This means that simply

adding mass to the structure is not a rewarding solution. By adding bulk mass to the host, the effect is minimal and a slight change in the natural frequencies is observed. However, adding the same amount of mass but in a metastructure manner (i.e. host + local absorbers) shows very promising effects. The linear analysis has been extensively investigated and therefore, the study is extended to the nonlinear regimes.

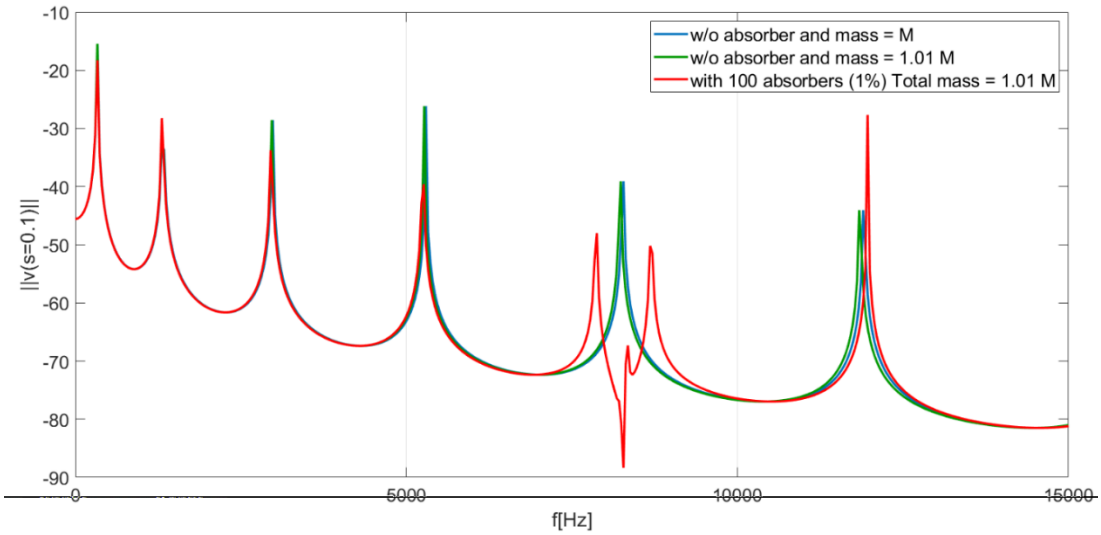

Figure 3.5: Frequency-response function of increasing the bulk mass of the beam by 1% (green) vs. adding 1% absorbers to the original beam (red)

Chapter 4. Nonlinear Response of the Metamaterial Beam

The previous chapter was totally devoted to the linear dynamic analysis of the metamaterial beam. However, in reality, there are sources of geometric nonlinearities in the host beam or in the absorbers. The analytical approach used in the linear analysis to generate the frequency response cannot be implemented in the subsequent study. Therefore, a space discretization approach, namely Galerkin's decomposition method, will be followed to obtain the nonlinear dynamic response.

Similar to the study presented in the preceding section, the nonlinear response of the metamaterial host (beam) is first investigated without adding any absorbers to the structure. This is to establish the baseline case for any analysis conducted hereafter.

4.1. Nonlinear Response: Single Bending Mode Without Absorbers

In this section, the simulation results based on a single bending mode (without absorbers) are shown. Initially, the beam mode shape is used to discretize the original governing equation and transform it to a nonlinear ordinary differential equation as given below:

$$\int_0^1 \phi_1^2\, ds\ \ddot{q}_1 + 2\zeta \int_0^1 \phi_1^2\, ds\ \dot{q}_1 + \int_0^1 \phi_1 \phi_1''''\, q_1 - \lambda^2 \left[\int_0^1 \phi_1 \phi_1'' \cdot \int_0^1 \frac{1}{2}(\phi_1)^2\, ds\right] q_1^3 = \int_0^1 f_2 \cdot \phi_1\, ds \tag{4.1}$$

Note the presence of a cubic nonlinearity q_1^3 that arises from the mid-plane stretching of the beam. Again, Eq. (4.1) is not coupled to any absorber. In this case, one needs to find the solution for only one generalized coordinate, namely, q_1. The parameters of the discretized beam equation has the following numerical values:

$$\int_0^1 \phi_1^2 = 1 \qquad \zeta = 1\% \qquad \frac{\pi^2\lambda^2}{2} = 2972.4 \qquad \int_0^1 \phi_1 \phi_1'''' = \omega^2 = \pi^4$$

By employing the preceding parameters into the Mettler model, the equation reads as

$$\ddot{q}_1 + 0.02\, \dot{q}_1 + \pi^4\, q_1 + 2972.4\, q_1^3 = f \cos\left((\pi^2 + \sigma) \cdot t\right) \tag{4.2}$$

Inspecting Eq. (4.2), we note that the equation is a second order ordinary differential equation. The equation is nonlinear due to presence of cubic terms.

Moreover, the equation is nonhomogeneous due to presence of forcing term (harmonic). Finally, the natural frequency is $\omega^2 = \pi^4$.

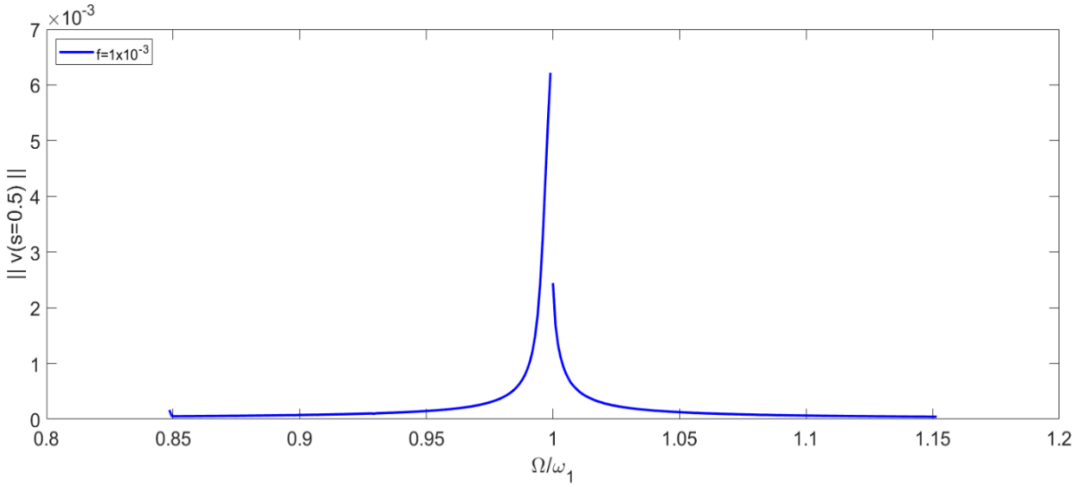

Figure 4.1: Frequency-response of the metamaterial beam near the primary resonance.

The forcing term has two parameters: the amplitude f and the tuning σ which indicates the nearness of the excitation frequency to the first natural frequency.We plot in Figure 4.1 the frequency response in the vicinity of the first natural frequency when setting the amplitude f equal to 1×10^{-3}. The frequency response is obtained by solving numerically Eq. (4.2) and reporting the maximum amplitude of the center of the beam for each excitation frequency. We explain here how the frequency response is obtained. Figure 4.2a shows the time history for a fixed amplitude and excitation frequency. In this case, the amplitude f is equal to 5×10^{-3} and the tuning parameter σ is set to 0. The simulation time is extended to allow the oscillations reaching its limit cycle (steady state solution). The amplitude of the steady-state solution is captured and is considered to be the point to plot in the frequency response. This point is shown in the cursor in Figure 4.2. Numerically from Figure 4.2, $\sigma = 0$ and $q_1(t)\ as\ t \rightarrow \infty = 0.007204$.

Recall, $\phi(0.5) = \sqrt{2}\sin(\pi \cdot 0.5)$. If we multiply $q_1(\infty) \times \phi(0.5) = v(s = 0.5) = 0.01018$. This point corresponds to a single point in the frequency response curve. At ω_1 and $\sigma = 0$ (middle), this point can be seen in Figure 4.2b. This value is taken as the initial condition when gradually changing the excitation frequency and solving the discretized equation. In this case, the tuning parameter becomes 0.01 and

the amplitude does not vary. The same process is looped again until eventually plotting all the points of the frequency response as shown in Figure 4.2b.

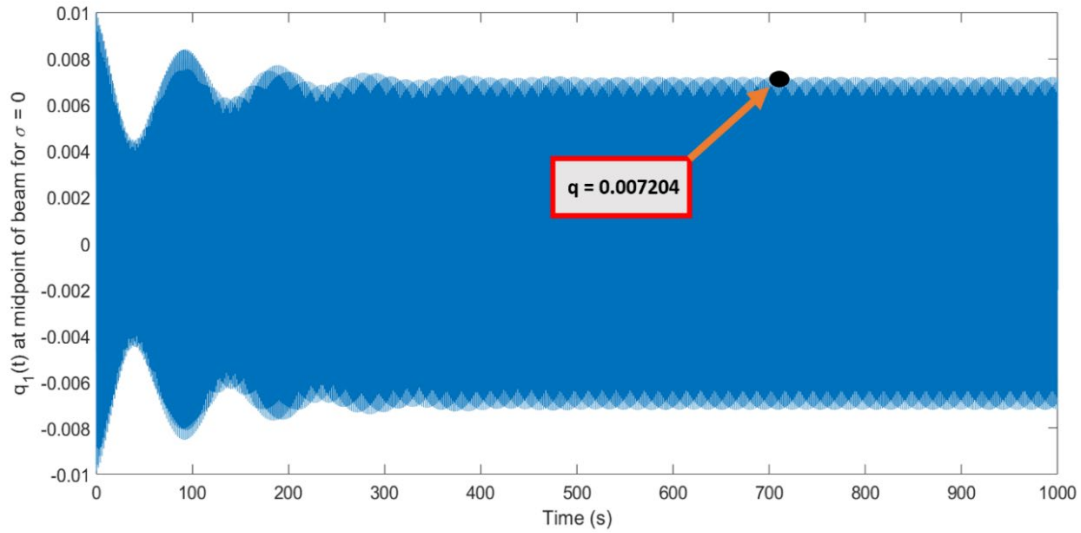

(a)

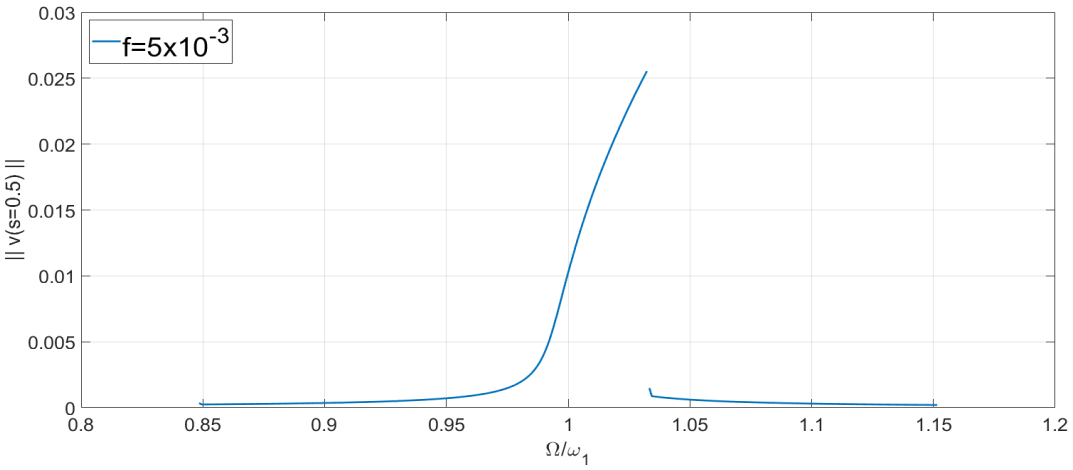

(b)

Figure 4.2: (a) Time history of q_1 for $f = 5 \times 10^{-3}$, $\sigma = 0$ and (b) the corresponding frequency response function at midpoint of beam.

As can be observed in Figure 4.1, the frequency response shows nearly-linear behavior. The graph is almost symmetrical and reaches its peak when the driving frequency is equal to the first natural frequency. Nonlinear characteristics can be seen such as the jump phenomena. Next, we will investigate the impact of increasing the forcing amplitude on the frequency response.

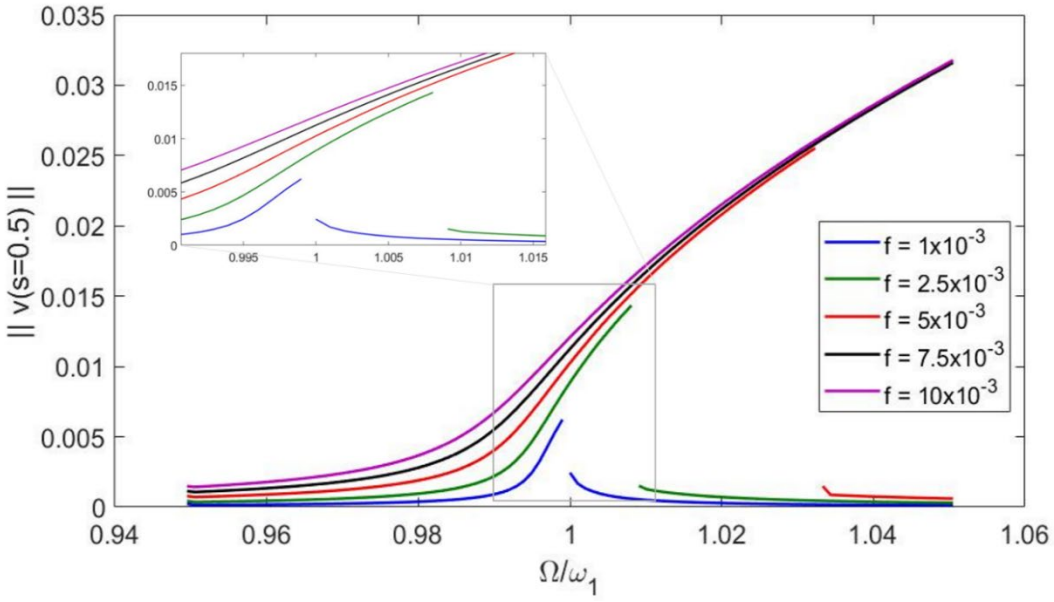

Figure 4.3: Frequency-response of the metamaterial beam for varying beam amplitudes

Figure 4.3 illustrates the effect of increasing the amplitude of the forcing term on the frequency response. The amplitude is varied from 1×10^{-3} to 10×10^{-3}. As expected, the curves are shifted to higher values as the amplitude is increased. We observe a clear tilt to the right resulting from the hardening effect, which is the manifestation of the geometric nonlinearity. Increasing the amplitude to 2.5×10^{-3},the nonlinear effect leads to a jump in the stable solutions. The amplitude is still relatively low and the nonlinear impact starts on coming into role. Increasing further the amplitude of the forcing term to 5×10^{-3} yields the occurrence of a frequency range over which no stable solution can be obtained from long time integration. Moreover, we observe a significant shift in the peak to higher amplitude. The peak is also shifted to the right of the natural frequency due to the significant impact of the cubic nonlinearity. The frequency response for the amplitude of 7.5×10^{-3} (denoted by the black line) shows similar trend with higher amplitudes. Setting the amplitude of the forcing term equal to 10×10^{-3}results in large jump in the stable dynamic solution. This constitutes an undesirable effect that may lead to the failure of the structure.

A family of frequency-response curves for various levels of load amplitude are presented in Figure 4.3. When the load amplitude is low, the frequency response

exhibits linear behavior with the peak amplitude of the motion taking place in close proximity to the natural frequency. By increasing the amplitude, the frequency-response curves tend to be bent to the right and exhibit a multi-valued range with hysteresis. The bandwidth of the multi-valued frequency range increases with the amplitude. The bending of the frequency-response curves to the right is the manifestation of the hardening nature of the geometric nonlinearity. Next, the effect of incorporating absorbers to the host structure (beam) is studied in the nonlinear regime. The main goal is to investigate the potential use of the absorbers to suppress the vibration of the main structure when being subject to high external loading.

4.2. Nonlinear Response: Multi Modes with Absorbers

After gaining insight on the system response without absorbers, we proceed with the simulation of the behavior of the metamaterial beam equipped with local resonators. To do so, we integrate the fully-coupled system given by Eqs. (2.44) and (2.45) expressed as

$$\int_0^1 \phi_k \left\{ \sum_{j=1}^{N_m} \left[\ddot{q}_j \phi_j + 2\zeta \dot{q}_j \phi_j + q_j \phi_j'''' - \lambda^2 q_j \phi_j'' \int_0^1 \frac{1}{2} \left(q_j \phi_j\right)^2 ds - f_2(s,t) \right] + \sum_{i=1}^{N_{va}} \mu_i \left[\sum_{j=1}^{N_m} \ddot{q}_j \phi_j(s_i) + \ddot{y}_i \right] \delta(s - s_i) \right\} ds = 0$$

$$\mu_i \left[\sum_{j=1}^{N_m} \ddot{q}_j \phi_j(s_i) + \ddot{y}_i \right] + 2\zeta_i \alpha_i \bar{\omega} \dot{y}_i + \mu_i \alpha_i^2 \bar{\omega}^2 y_i + N_i(y_i^2, y_i^3) = 0$$

The different parameters shown in the above equation are introduced and defined in Chapter 2. We conduct a parametric study to show the impact of the number and location of the absorbers on the level of vibration suppression of the main structure. We consider a numerical example to simulate the dynamic behavior of the beam using 2 bending modes and 2 absorbers. We start with a small number of generalized coordinates to gain insight of the dynamic behavior and then extend the set of equations to larger number of absorbers and modes. The obtained equations of motion are shown below

$$\int_0^1 \phi_1^2 \; \boldsymbol{ds} \; \ddot{\boldsymbol{q}}_{\boldsymbol{1}} + \int_0^1 \phi_1\phi_2 \, ds \, \ddot{\boldsymbol{q}}_{\boldsymbol{2}}$$
$$+ 2\zeta \int_0^1 \phi_1^2 \, ds \; \dot{\boldsymbol{q}}_{\boldsymbol{1}} + 2\zeta \int_0^1 \phi_1\phi_2 \, ds \; \dot{\boldsymbol{q}}_{\boldsymbol{2}}$$
$$+ \int_0^1 \phi_1\phi_1'''' \; ds \; \boldsymbol{q}_{\boldsymbol{1}} + \int_0^1 \phi_1\phi_2'''' \; ds \; \boldsymbol{q}_{\boldsymbol{2}}$$
$$- \frac{\lambda^2}{2}\left[\int_0^1 \phi_1\phi_1'' \cdot \int_0^1 \phi_1^2\right] \boldsymbol{q}_{\boldsymbol{1}}^{\boldsymbol{3}} - \frac{\lambda^2}{2}\left[\int_0^1 \phi_1\phi_2'' \cdot \int_0^1 \phi_2^2\right] \boldsymbol{q}_{\boldsymbol{2}}^{\boldsymbol{3}}$$
$$+ \mu_1 \int_0^1 \phi_1^2 \, \delta\,(s - s_1) \, \ddot{\boldsymbol{q}}_{\boldsymbol{1}}$$
$$+ \mu_1 \int_0^1 \phi_1\phi_2 \, \delta\,(s - s_1) \, \ddot{\boldsymbol{q}}_{\boldsymbol{2}}$$
$$+ \mu_1 \int_0^1 \phi_1 \, \delta\,(s - s_1) \ddot{\boldsymbol{y}}_{\boldsymbol{1}} + \mu_2 \int_0^1 \phi_1^2 \, \delta\,(s - s_2) \, \ddot{\boldsymbol{q}}_{\boldsymbol{1}}$$
$$+ \mu_2 \int_0^1 \phi_1\phi_2 \, \delta\,(s - s_2) \, \ddot{\boldsymbol{q}}_{\boldsymbol{2}}$$
$$+ \mu_2 \int_0^1 \phi_1 \, \delta\,(s - s_2) \; \ddot{\boldsymbol{y}}_{\boldsymbol{2}} = \int_0^1 \phi_1 \, f_2 \, ds$$

$$\int_0^1 \phi_1\phi_2 \; \mathrm{ds} \; \ddot{\mathbf{q}}_{\mathbf{1}} + \int_0^1 \phi_2^2 \, \mathrm{ds} \, \ddot{\mathbf{q}}_{\mathbf{2}}$$
$$+ 2\zeta \int_0^1 \phi_1 \, \phi_2 \, \mathrm{ds} \; \dot{\mathbf{q}}_{\mathbf{1}} + 2\zeta \int_0^1 \phi_2^2 \, \mathrm{ds} \; \dot{\mathbf{q}}_{\mathbf{2}}$$
$$+ \int_0^1 \phi_2\phi_1'''' \; \mathrm{ds} \; \mathbf{q}_{\mathbf{1}} + \int_0^1 \phi_2\phi_2'''' \; \mathrm{ds} \; \mathbf{q}_{\mathbf{2}}$$
$$- \frac{\lambda^2}{2}\left[\int_0^1 \phi_2\phi_1'' \cdot \int_0^1 \phi_1^2\right] \mathbf{q}_{\mathbf{1}}^{\mathbf{3}} - \frac{\lambda^2}{2}\left[\int_0^1 \phi_2\phi_2'' \cdot \int_0^1 \phi_2^2\right] \mathbf{q}_{\mathbf{2}}^{\mathbf{3}}$$
$$+ \mu_1 \int_0^1 \phi_2\phi_1 \, \delta\,(s - s_1) \, \ddot{\mathbf{q}}_{\mathbf{1}}$$
$$+ \mu_1 \int_0^1 \phi_2^2 \, \delta\,(s - s_1) \, \ddot{\mathbf{q}}_{\mathbf{2}}$$
$$+ \mu_1 \int_0^1 \phi_2 \, \delta\,(s - s_1) \, \ddot{\mathbf{y}}_{\mathbf{1}} + \mu_2 \int_0^1 \phi_2\phi_1 \, \delta\,(s - s_2) \, \ddot{\mathbf{q}}_{\mathbf{1}}$$
$$+ \mu_2 \int_0^1 \phi_2^2 \, \delta\,(s - s_2) \, \ddot{\mathbf{q}}_{\mathbf{2}}$$
$$+ \mu_2 \int_0^1 \phi_2 \, \delta\,(s - s_2) \; \ddot{\mathbf{y}}_{\mathbf{2}} = \int_0^1 \phi_2 \, f_2 \, \mathrm{ds}$$

$$\mu_1\phi_1\,(s_1)\,\ddot{\boldsymbol{q}}_{\boldsymbol{1}} + \mu_1\,\phi_2(s_1)\,\ddot{\boldsymbol{q}}_{\boldsymbol{2}} + \mu_1\,\ddot{y}_1 + 2\zeta_1\mu_1\alpha_1\bar{\omega}\,\dot{\boldsymbol{y}}_{\boldsymbol{1}} + \mu_1\alpha_1^2\bar{\omega}^2\,\boldsymbol{y}_{\boldsymbol{1}} = 0$$

$$\mu_2\phi_1\,(s_2)\,\ddot{\boldsymbol{q}}_{\boldsymbol{1}} + \mu_2\,\phi_2(s_2)\,\ddot{\boldsymbol{q}}_{\boldsymbol{2}} + \mu_2\,\ddot{\boldsymbol{y}}_{\boldsymbol{2}} + 2\zeta_2\mu_2\alpha_2\bar{\omega}\,\dot{\boldsymbol{y}}_{\boldsymbol{2}} + \mu_2\alpha_2^2\bar{\omega}^2\,\boldsymbol{y}_{\boldsymbol{2}} = 0 \quad (4.3)$$

We note that the generalized coordinates and their time derivatives are shown in **bold** and they are preceded with the coefficient needed to be computed. Given the orthogonality condition of the mode shapes, the integral $\int_0^1 \phi_1\,\phi_2$ vanishes.

The following numerical values of the parameters and conditions are used to simplify the equations above

$$\int_0^1 \phi_k^2 = 1, \qquad \int_0^1 \phi_1\,\phi_2 = 0, \quad \zeta = 0.01, \qquad \frac{\lambda^2\cdot\pi^2}{2} = 2972.4, \quad \mu_1 = \mu_2 = 0.005,$$

$$\alpha\,\bar{\omega} = 78.622\,\pi = 247, \qquad s_1 = \frac{1}{3}\;s_2 = \frac{2}{3}, \qquad l = 1m \quad \phi_n(s) = \sqrt{2}\sin\left(\frac{\pi}{l}\cdot s\right)$$

After evaluating and computing the preceding equations, the following set of nonlinear equations are obtained:

$$1.015\,\ddot{q}_1 + 0.0061\,\ddot{y}_1 + 0.0061\,\ddot{y}_2 + 0.02\;\dot{q}_1 + \pi^4\,q_1 + 0.05\,q_1^3 = \;10\,cos\;[\,(9.8982+\sigma)\cdot t\,]$$

$$1.015\,\ddot{q}_2 + 0.0061\,\ddot{y}_1 - \;0.0061\,\ddot{y}_2 + 0.02\,\dot{q}_1 + (16\cdot\pi^4)\;q_1 + 0.5\,q_1^3 = \;10\,cos\;[\,(39.5390+\sigma)\cdot t\,]$$

$$0.0061\,\ddot{q}_1 + 0.0061\,\ddot{q}_2 + 0.005\,\ddot{y}_1 + 0.0247\,\dot{y}_1 + 304.3583\,y_1 = 0$$

$$0.0061\,\ddot{q}_1 - \;0.0061\,\ddot{q}_2 + 0.005\,\ddot{y}_2 + 0.0247\,\dot{y}_2 + 304.3583\,y_2 = 0 \quad (4.4)$$

We note that the nonlinear term of the kth mode equation in general is $\mathrm{k}^2\cdot\frac{\lambda^2\,\pi^2}{2} = \mathrm{k}^2\cdot 2972.4$

The obtained equations are not only coupled but also nonlinear. The equations are rewritten in state-space form as:

$$M\dot{y} + Cy + Kx + N - f = \;0$$

where $y = \dot{q}$

We introduce the state vector $z = [q\;y]'$ and consequently we obtain

$$\dot{z} = Az - \widetilde{N} + \tilde{f}$$

where $A = \begin{bmatrix} 0 & I \\ -M^{-1}K & -M^{-1}C \end{bmatrix}$, $\widehat{N} = \begin{bmatrix} 0 \\ -M^{-1}N \end{bmatrix}$, $\hat{F} = \begin{bmatrix} 0 \\ -M^{-1}F \end{bmatrix}$

The coefficients of the above matrices can be extracted from the below equations

$$\ddot{q}_1 = -97.4\, q_1 - 0.02\, \dot{q}_1 + 0.005\, q_1^3 + 371.27\, y_1 + 0.03\, \dot{y}_1 + 371.27\, y_2 + 0.03\, \dot{y}_2 - 10\cos(\omega_1)$$

$$\ddot{q}_2 = -1558.4\, q_2 - 0.02\, \dot{q}_2 - 0.5\, q_2^3 + 371.27\, y_1 + 0.03\, \dot{y}_1 - 371.27\, y_2 - 0.03\, \dot{y}_2 - 10\cos(\omega_2)$$

$$\ddot{y}_2 = 118.8\, q_1 + 0.024\, \dot{q}_1 - 1901.2\, q_2 - 0.024\dot{q}_2 - 61777\, y_2 - 5.0135\, \dot{y}_2 + 0.006\, q_1^3 - 0.61\, q_2^3 - 12.2\cos(\omega_1) + 12.2\cos(\omega_2)$$

$$\ddot{y}_1 = 118.8\, q_1 + 0.024\, \dot{q}_1 + 1901.2\, q_2 + 0.024\dot{q}_2 + 61777\, y_1 - 5.0135\, \dot{y}_1 + 0.006\, q_1^3 + 0.61\, q_2^3 + 12.2\cos(\omega_1) + 12.2\cos(\omega_2) \quad (4.5)$$

The set of coupled nonlinear equations are solved numerically using the Matlab tool ode45.

Proceeding with the nonlinear analysis, the effect of embedding local resonators to the main host is studied. The ratio of the mass of the absorber to the mass of the host is $= 1\%$. Moreover, this extra mass is divided upon the number of absorbers. This means that each absorber will have a mass ratio of $\mu_i = \frac{\mu}{N_a}$. The crucial parameter here is the frequency each absorber is tuned at and its effect on the response of the host. As mentioned before, our target is mitigating the amplification in the vicinity of the first three fundamental modes. These are the most dominating modes.

4.3. Case studies: Effect of Local Absorbers Distribution

Three different scenarios are implemented and studied. A summary of the three different cases is given in Table 4.1 In the three different scenarios, nine absorbers are embedded to the host. However, the absorbers were tuned at different frequencies for the different case tudies. The response of each case is thoroughly investigated. One should note what is being calculated is the displacement of the host's midpoint. However, for the frequency response in the neighborhood of the second natural frequency, the displacement in the middle of the beam is always zero. As such. the

displacement is computed at quarter the beam (s=0.25) when the forcing term is excited near the second mode.

The frequency response curves obtained with and without absorbers are displayed in Figure 4.4 as per the cases described in Table 4.1. We simulate the dynamic response in the vicinity of the first three natural frequencies. The baseline scenario corresponds to the response of the host without any absorbers (denoted by the blue curve). In the neighborhood of the first three natural frequencies, we observe high amplitudes and significant jump in the stable solutions as discussed in the previous section. This is the unmitigated host metamaterial beam. The x-axis is normalized with the natural frequency of the first three modes.

Table 4.1: Breakdown of nine absorbers (tuning frequency) in each case

	ω_1	ω_2	ω_3
CASE 1	9	0	0
CASE 2	3	3	3
CASE 3	6	2	1

Next, we analyze each case separately and show the potential vibration suppression of the host structure. This parametric study aims at providing guidelines to control the large vibrations of the host structure based on the operating frequency range of the external loading.

4.3.1. Case 1 (9-0-0). Moving on with the analysis, in Case 1, all the nine absorbers are tuned entirely to the first mode. As Figure 4.4 (a) shows, the vibration is mitigated near the first mode only. The second and third natural modes are barely affected as seen in Figure 4.4 (b) and (c), and the nonlinearity still dominates the dynamic behavior. This case is a simple condition where all the local absorbers are tuned to the first mode. Hence, only the first mode is controlled whilst the second and third mode turn out to be nearly uncontrolled. The effect of the tuned absorbers on the first mode, though, is notable. The peak is highly suppressed, and the nonlinear effects diminish. Nevertheless, our aim, is to mitigate the amplitude of motion in the vicinity

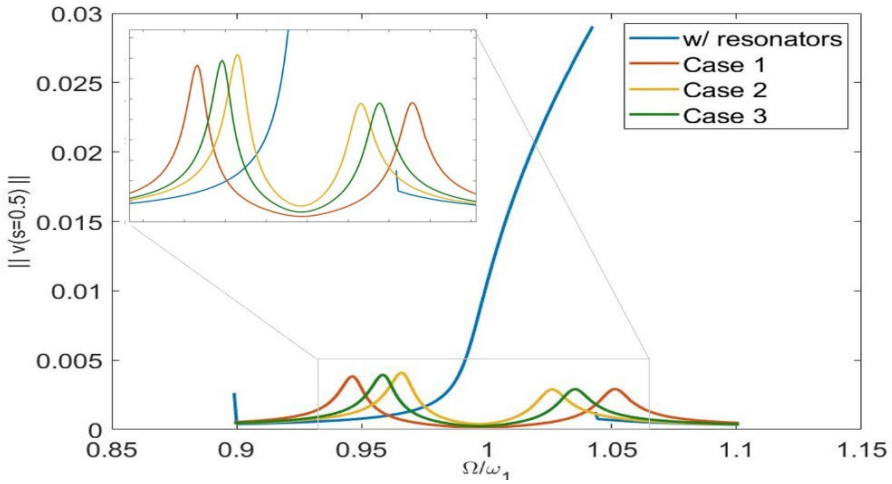

(a)

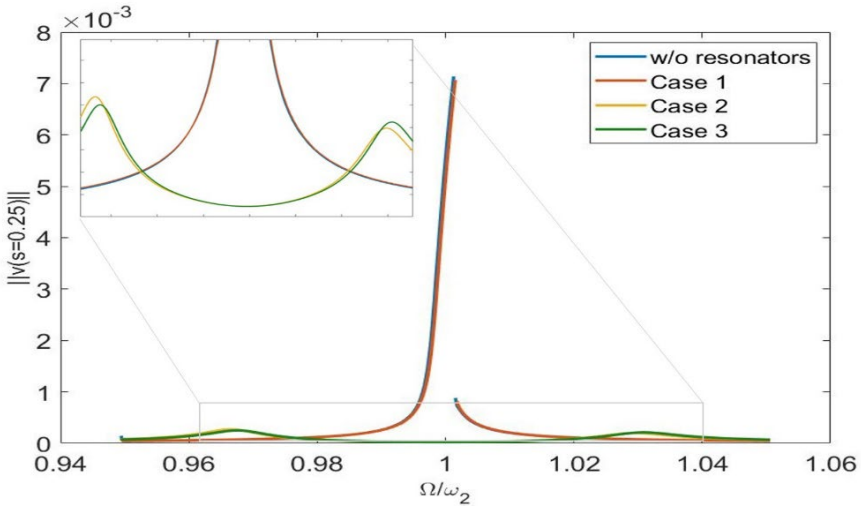

(b)

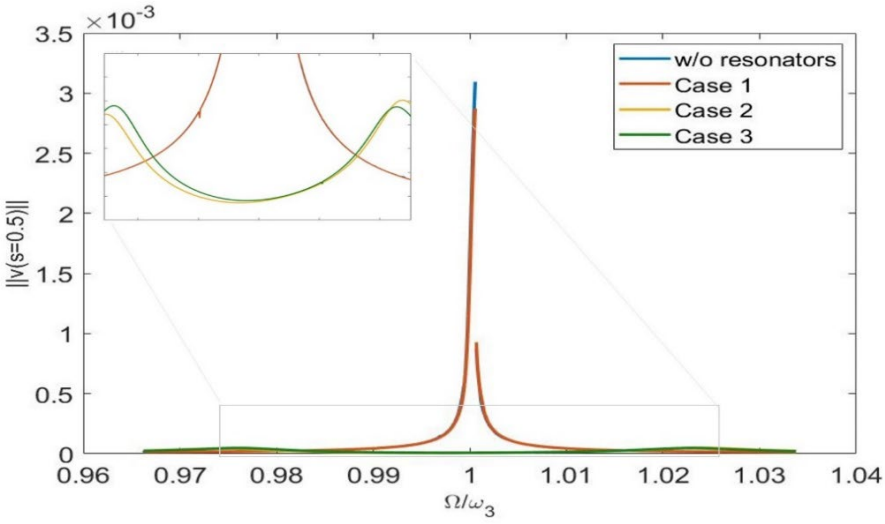

(c)

Figure 4.4: The frequency-response curves of the beam around the first three natural frequencies

of the first three modes simultaneously. This is where the role of tuning each absorber separately comes into play.

4.3.2. Case 2 (3-3-3). In Case 2, the nine absorbers are tuned in a pattern to cover the lowest three bending modes. The first set (three resonators) are tuned to the first, second and third modes, respectively. This pattern is extended to the second and third set of absorbers. This mean the first, fourth and seventh absorbers are tuned to the first mode and so on. The second, fifth and eights absorbers are tuned to the second mode. The rest are tuned to the third mode. Hence, three absorbers are devoted for each mode. The effect of the absorbers is observed in the three modes. However, the first mode experiences a decrease in the bandwidth of mitigation. The number of absorbers and the total mass of resonators devoted to the first mode is less compared to the first case. The amplitudes are still suppressed but the range of operation is reduced. Slight peaks are observed near the second and third modes. Nevertheless, the second and third modes are almost fully mitigated. This is because as the modes progress, the effect of the subsequent modes become less prominent and it becomes easier to suppress the higher modes with the same number of absorbers as the first mode. The conclusion one can draw from this simulation case is that the first mode excites a considerable amount of the beam mass and is characterized by larger amplitudes. On the contrast, the second and third modes are not as dominant as the first mode and they require less absorbers (compared to the first mode) to notice the effect of mitigation. Therefore, it is convenient to adopt a different tuned frequency distribution along the absorbers. This is discussed in the last scenario (Case 3).

4.3.3. Case 3 (6-2-1). In Case 3, the nine absorbers are tuned in a biased way. Since the hardest mode to suppress is the first fundamental mode, more absorbers are tuned to the first natural frequency. Precisely, 66.67% are devoted to the first mode, while the second and third modes are devoted by 22.2% and 11.11% of the absorber mass, respectively. These percentages in particular are not based on any particular calculation. The percentages are taken from the previous work by Casalotti et al. [55]. This configuration allows us to have a better region of operation of the first mode whilst keeping the second and third modes still under control. This is apparent in Figure 4.4 where the bandwidth of the first mode increases and the amplitudes of vibration are significantly reduced near the second and third modes. As expected, the second and

third modes show similar behavior as obtained in Case 2. The magnitude of the dynamic solution is significantly reduced used only few absorbers tuned at the second and third modes. On the other hand, the first mode needs more absorbers to suppress the large vibrations obtained when exciting the host near the first natural frequency. Case 3 demonstrates the importance of the distribution of the absorbers and selection of their tuning frequencies to achieve multi-mode vibration suppression. As such, we formulate in the subsequent chapter an optimization problem to explore the possible further enhancement in terms of vibration suppression by tuning appropriately the frequencies of the absorbers.

4.4. Response of the Absorbers

The preceding results showed the promising effect of the absorbers in suppressing the vibration of the host structure. On the other hand, there should be some kind of trade off. In this situation, the suppression of vibration of the host beam occurs at the expense of the excitation of the local absorbers. Figure 4.5 shows the frequency response of the metamaterial beam and the response of the single absorber embedded to it at the midpoint. As usual, the blue curve shows the response of the host beam without absorbers. Moreover, the green plot shows the frequency response of the midpoint of the host beam. The mitigation of the host structure is greatly achieved. Nevertheless, the absorber undergoes vibrations with amplitude much greater than that of the host structure.

Despite the absorber showing high amplitudes in Figure 4.5, the highest peaks are found a bit further from the frequency response. This gives the frequency a wider bandwidth. In fact, the use of a single absorber may lead to an optimum control. However, it suffers from practical limitations and drawbacks due to mass concentration. In Figure 4.5, the extra mass 1% is completely added by just a single absorber. This creates a concentrated point force acting on the beam. This relatively huge mass can lead to high stress concentration in the region of contact. Therefore, the use of higher number of absorbers is preferable.

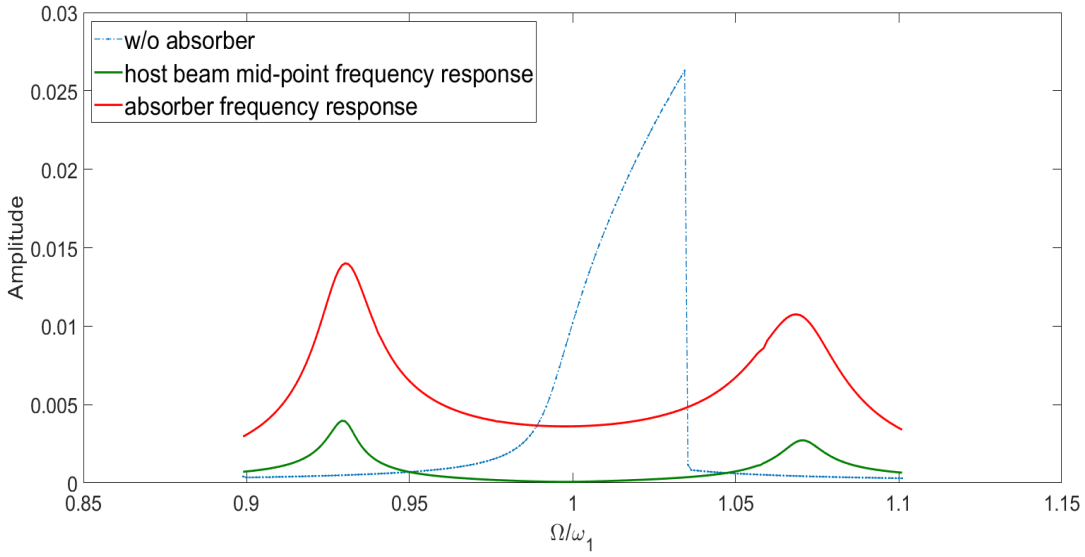

Figure 4.5 Comparison between frequency response of the host beam and the absorber at mid-span.

Chapter 5. Optimization of the Nonlinear Metamaterial Beam Response

The analyses presented in the previous chapters revealed that integrating local absorbers to a host in a metastructure fashion greatly suppresses the vibration when being subject to external loading excited near its resonance. Precisely, our main goal was to mitigate the vibrations occurring in the vicinity of the first three natural frequencies. Moreover, the preceding section showed that amongst the first three natural modes, the first mode required more number of absorbers to secure the vibration suppression when operating near the first natural frequency. The need to devote more absorbers to be tuned to the first mode is clear. However, the optimal frequency to be tuned to and its spatial location is not apparent. In addition, the number of absorbers can play a role in enhancing the mitigation of the large vibrations. We note that increasing the number of absorbers does not add extra mass to the host since the mass ratio μ is maintained constant. The number of absorbers and their tuned frequencies along with the spatial location of these tuned frequencies can all be modulated to further suppress the large vibrations obtained near resonance. We explore this by formulating an optimization problem with the objective to maximize the reduction in the amplitude of vibrations while varying some control parameters.

5.1. Optimization Tool: Pattern Search Algorithm

The Matlab tool based on the optimization pattern search algorithm [64] is combined with the developed code to generate the nonlinear frequency response of the metamaterial beam. We define the objective function as the area underneath the frequency-response curve over the frequency bandwidth of $\pm 10\%$ the natural frequency of each considered mode. The objective function is evaluated using the proposed numerical model. The control parameter considered in this study is the tuning frequencies of the absorbers. Below we give some background on the optimization algorithm implemented on Matlab.

According to [64], pattern search can be used to minimize a real-valued function

$$minimize\ f(x), where\ x\ \in R^n$$

Pattern search algorithm directs the search for a minimum through a pattern containing at least n+1 points per iteration, where the vectors representing the direction and

distance of each point relative to the current iterate from a positive bases in R^n. Furthermore, an iteration of a pattern search algorithm may require as few as one function evaluation because the search requires only simple decrease to accept a new point. In that way, even large patterns may be used sparingly.

The pattern search algorithm used here is a built-in function in Matlab. By default, patter search looks for a minimum based on an adaptive mesh. To implement the function, all parameters are fixed such as number of absorbers/modes, host mass, mass ratio of absorbers, etc. The only control parameter is the tuning frequency. Consequently, the objective function developed has only one varying input. This objective function is the area under the frequency-response curve within $\pm$ 10% in the vicinity of the first mode. The main goal is to identify the optimal tuning frequencies of the absorbers minimizing the aforementioned objective function.

We first fix the number of absorbers and consider the only variable that can be modulated to be the tuned frequency of each absorber. We note that the range of the tuning frequencies is taken [0 400] Hz. The optimizer searches for the values of these frequencies leading to reduction in the objective function. The Matlab command is given below

$$alphaopt = patternsearch\ (@objective, alpha0, A, b, Aeq, beq, lb, ub)$$

where one needs to define a set of lower and upper bounds on the control variable α (tuning frequency), so that the search of the optimal values is performed within the range $lb < alpha < ub$. The Aeq = [] and beq = [] since no additional constraints are introduced to the optimization problem. $alpha0$ is the initial guess of the control parameter. The choice of is critical to speed up the search of the local optimizer of the optimal tuning frequency. With this brief overview of the optimizer deployed in the present study, the optimization results are presented and discussed in the next section.

5.2. Optimization Results

We consider a simple configuration based on a host structure equipped with only one absorber and being excited near its primary resonance. By intuition, since the target is to maximize the vibration suppression near the primary resonance, this single absorber would be tuned at exactly the first natural frequency; that is, 330.825 Hz as shown in Table 3.1. We run the optimizer while taking an initial guess of 100 Hz. Of

interest, the optimizer identified a tuning frequency of 327.5 Hz. This indicates that if the only absorber is tuned to this frequency, the area underneath the frequency-response curve within the considered frequency bandwidth is minimized. We plot in Figure 5.1 the frequency response obtained without absorbers (baseline case) and with one absorber while setting its tuning frequency at the first natural frequency (Case 1) and at the optimal one (Case 2). The objective function (area beneath the curve within the frequency bandwidth) calculated without embedding any absorbers is found equal to 8.8446×10^{-3}. When the absorber is tuned to the first mode frequency 330.825 Hz, the area is significantly decreased to reach 2.4479×10^{-3}. More interestingly, when the absorber is tuned to the optimal frequency 327.5 Hz, the area beneath decreased to around 2.3442×10^{-3}. This constitutes an overall decrease in the objective function to about 73.4%.

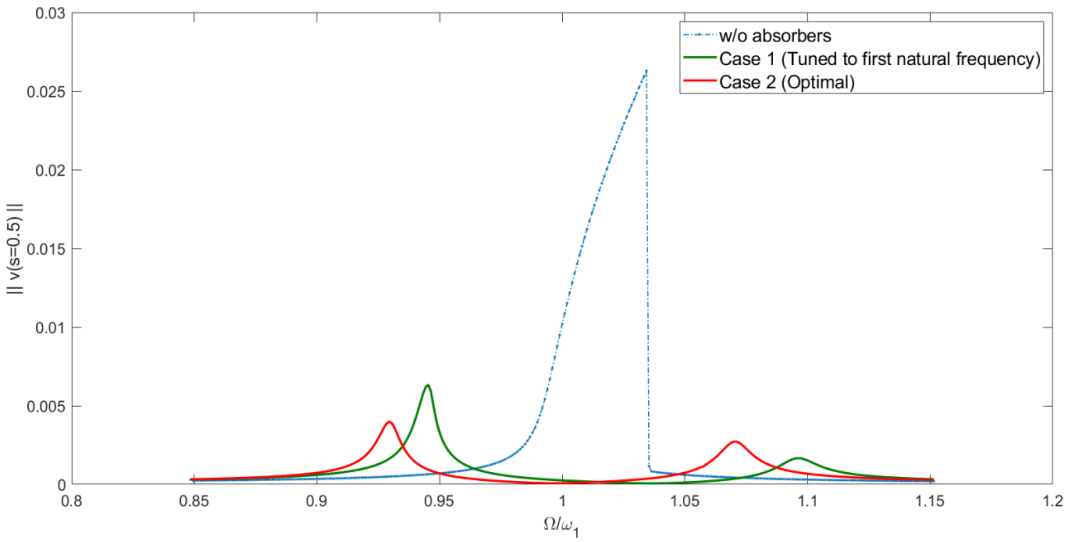

Figure 5.1: Frequency response of metamaterial beam optimized for 1 mode + 1 absorber

In practical terms, this decrease in area is mostly influenced by the decrease of the response peak. Without absorbers, the midspan of the host vibrates with an amplitude of 0.025 m. By adding one absorber with $f_1 = 330.825$ Hz, the highest peak is 0.007 m. On the other hand, by modulating the absorber to $f_{1_{opt}} = 327.5\, Hz$, the highest peak does not exceed 0.005m. For a simple case, the further reduction of area (i.e., from Case 1 to Case 2), may not be very pronounced. Nevertheless, by increasing

the number of absorbers, the results can become even more interesting. The number of modes and absorbers are now increased.

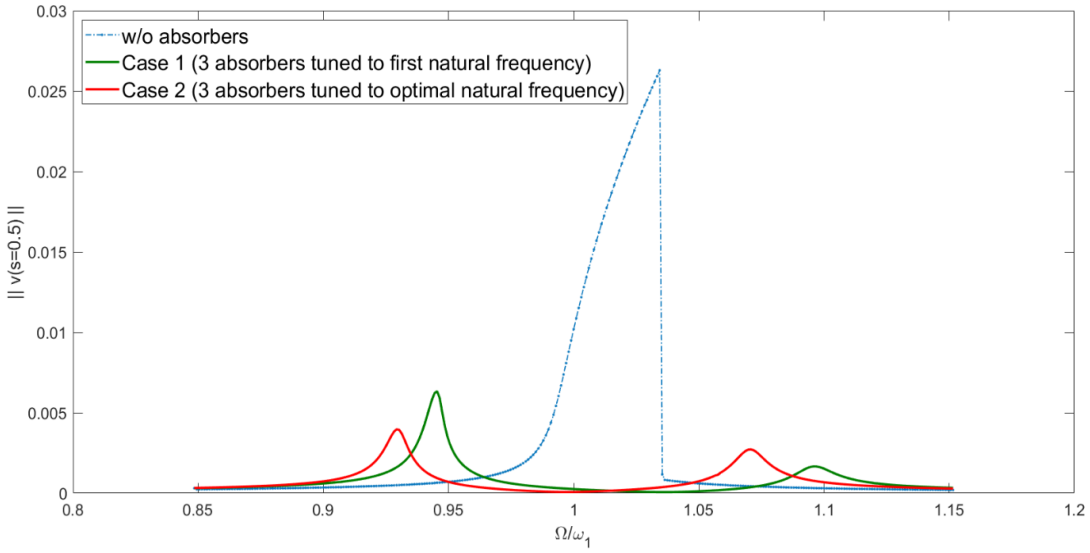

Figure 5.2: Frequency response of metamaterial beam optimized for 3 modes + 3 absorbers

The second optimization case is conducted using three modes while equipping the host structure with three absorbers. The same aforementioned procedure is followed. Figure 5.2 shows the frequency response curves of host structure with and without absorbers. The area under the curve within the considered frequency bandwidth is the same as the single mode response for the baseline case which is 8.8446×10^{-3}. Next, the three absorbers are all tuned to the first natural frequency; that is, $f_{abs_1} = f_{abs_2} = f_{abs_3} = f_1 = 330.825\ Hz$. The area decreases to 2.0285×10^{-3} as shown in Figure 5.2. Nevertheless, as shown in the previous case (single mode), the optimal frequencies will be slightly higher or lower than the exact natural frequency due to the inherent system's nonlinearities. The optimizer identified a set of frequencies leading to a further decrease in the objective function. The area reaches 1.5002. This represents an area reduction of 73.7% of the original unmitigated beam. Moreover, this is a further 25% decrease of the intuitive case (Case 1). The obtained optimal frequencies are $f_{abs_1} = 314.3\ Hz, f_{abs_2} = 359.6\ Hz, f_{abs_3} = 335.1\ Hz$.

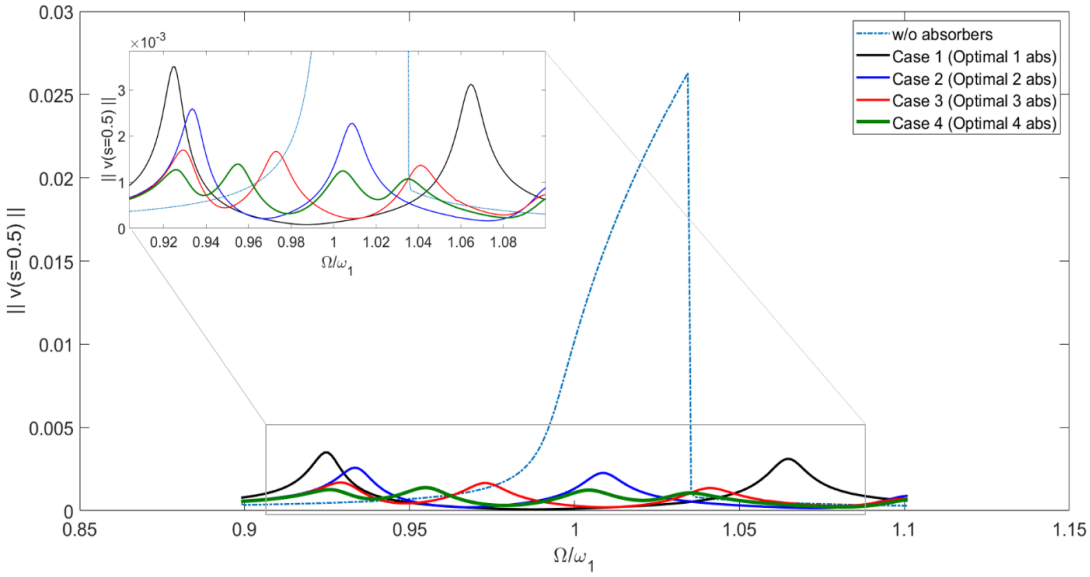

Figure 5.3: Frequency response of metamaterial beam optimized for varying number of absorbers

It is clear that the optimization study gives promising results and by modulating the absorbers slightly higher or lower than the natural frequency leads to higher mitigation levels. The preceding two cases show that optimization enables better selection of the tuning frequencies even for the straightforward cases. Henceforth, we investigate the number of absorbers needed to achieve a notable mitigation of the vibration of the absorbers.

The final analysis presented here is the effect of the number of absorbers on the mitigation of the host in the vicinity of the first natural frequency. As apparent from the previous discussion, optimization yields promising mitigation levels. Henceforth, from this point onwards, whatever the number of absorbers is, they are all tuned to the optimal frequency identified by the optimizer and not the first natural frequency $f_1 = 330.825\ Hz$. Figure 5.3 shows the frequency response curves obtained for the optimal cases for varying number of absorbers. The number of absorbers is increased from one to four. The optimal frequencies of each mode along with their objective function (area under the frequency response curve) are presented in Table 5.1. A significant reduction in the objective function is obtained even using only one absorber tuned at slightly lower than the first natural frequency of the host structure. About 83% reduction in the

objective function is achieved when deploying four absorbers. This indicates the usefulness of the local absorbers to suppress the vibrations of the host structure.

Table 5.1 Summary of optimal frequency of each absorber along with the area under the graph

Number of absorbers	ω_{va_1}	ω_{va_2}	ω_{va_3}	ω_{va_4}	Objective function $\times 10^{-3}$
0	-	-	-	-	8.8446
1	327.5	-	-	-	1.9131
2	315.5	343.2	-	-	1.6007
3	314.3	359.6	335.1	-	1.5002
4	310.2	333.3	321.3	334.6	1.447

As shown in Figure 5.3, the addition of each absorber leads to further suppression of the oscillations amplitude. Increasing the number of absorbers from 1 (Case 1) to 4 (Case 4) results in reduction in the area under the frequency-response curve within the frequency bandwidth of almost 24%. The area drops from 8.8446×10^{-3} to an astonishing 1.447×10^{-3}. This is a very intriguing result since the amplification of the first mode is almost flattened as much as the second and third modes with only four absorbers. The highest peaks in Case 1 reaches 0.004 which is a good decrease in the amplification by itself. Nevertheless, increasing the number of absorbers to two, the area was further reduced. Three absorbers gave better results than two absorbers. Finally, the four absorbers seem to be flat and the highest peak is less than half of the first case. The investigation was halted at four absorbers because further addition of absorbers yields minor improvement in the vibration suppression.

It is worthy to note that if we investigate the results presented in Figure 5.3 more closely and we calculate the area underneath the frequency-response curve within ± 5 % the first natural frequency, the use of a low number of resonators, ideally, a single absorber, leads to the optimal control. However, it suffers from practical drawbacks due to the mass concentration (i.e point forces) in a few cross sections of the beam. It may not be possible to install the absorber masses because of geometric

limitations as well as huge masses can lead to failure of the retaining devices due to high stress concentrations in these regions. Figure 5.3. shows the response of one absorber compared to the response of four absorbers. That is why a higher number of resonators and a uniform mass distribution is preferable. The convergence and number of iterations of the optimizer based on the pattern search algorithm is shown in Figure 5.4 The convergence plot demonstrates the capability of the optimizer to find the optimal value of the tuning frequency with less than 40 iterations.

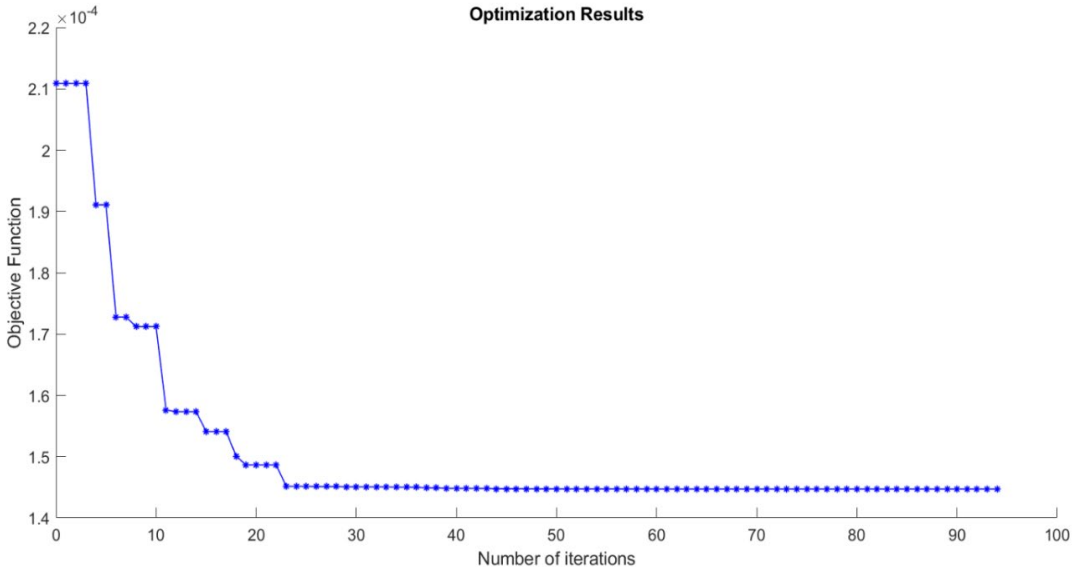

Figure 5.4: Convergence of the objective function based on the pattern search optimization algorithm.

Chapter 6. Conclusion and Future Work

6.1. Conclusion

In this thesis, metastructures are considered to reduce vibration of the host structure (beam) within a desired frequency. Metamaterials present a new class of semi-active composites. The aim of this work is to suppress the vibration of a host structure subject to external loading by utilizing metamaterial beam and yet, keeping the entire mass of the system. This means that the suppression of vibration should not come in the expense of added mass. To do so, the concept of a metamaterial beam, the mechanical metamaterial, embedded with local resonators (absorbers) has been investigated while accounting for the inherent geometric nonlinearities.

A coupled mathematical model was developed to simulate the nonlinear dynamic behavior of a simply-supported beam attached to an array of mass-spring systems acting as local absorbers. The present work aimed at analyzing how the tuning of local resonators can protect a beam-like structure from large vibrations due to external forcing. The effect of the absorbers on the nonlinear response of the beam in the vicinity of the first three natural frequencies were proved to be beneficial in terms of vibration suppression. The numerical results demonstrate that tuning more absorbers to the first mode in caparison to the subsequent modes is helpful to maintain acceptable vibration suppression levels and frequency bandwidth when operating near any of the first three natural frequencies.

Optimization results showed that further mitigation is possible. Tuning the absorber to the optimized values of frequency which are slightly less or more than the natural frequency showed pronounced results. The area underneath the frequency-response curve in the neighborhood of the first natural frequency was almost flattened. This demonstrates the usefulness of the absorbers to suppress the vibrations of the host structure.

6.2. Future Work

As future research work, nonlinearity will be added to the local absorbers and explore its impact on the level of vibration suppression. We will also perform multi-mode optimization analysis with the goal to select the tuning frequencies of the

absorbers while securing vibration suppression over wider frequency range including the first three natural frequencies. The multimode optimization will include the spatial position of each absorber as well. Since the damping ratios used in this study was relatively low, the effect of very high damping ratios will be studied. Moreover, the effectiveness of the absorbers will be tested under random excitation frequencies. This will be useful in case of large variation in the excitation frequency of the external loading such as seismic waves.

References

[1] Heyden and M. Ortiz, "Oncotripsy: Targeting cancer cells selectively via resonant harmonic excitation," *Journal of the Mechanics and Physics of Solids*, vol. 92, pp. 164–175, 2016.

[2] R. W. Ziolkowski and N. Engheta, "Introduction, History, and Selected Topics in Fundamental Theories of Metamaterials," *Metamaterials*, vol. 1, pp. 1–41.

[3] S. A. Cummer, J. Christensen, and A. Alù, "Controlling sound with acoustic metamaterials," *Nature Reviews Materials*, vol. 1, no. 3, pp. 1–13, 2016.

[4] D. R. Smith, W. J. Padilla, D. C. Vier, S. C. Nemat-Nasser, and S. Schultz, "Composite Medium with Simultaneously Negative Permeability and Permittivity," *Physical Review Letters*, vol. 84, no. 18, pp. 4184–4187, 2000.

[5] A. Alù and N. Engheta, "Plasmonic and metamaterial cloaking: physical mechanisms and potentials," *Journal of Optics A: Pure and Applied Optics*, vol. 10, no. 9, pp. 1–17, 2008.

[6] D. Schurig, J. J. Mock, B. J. Justice, S. A. Cummer, J. B. Pendry, A. F. Starr, and D. R. Smith, "Metamaterial Electromagnetic Cloak at Microwave Frequencies," *Science*, vol. 314, no. 5801, pp. 977–980, 2006.

[7] J. B. Pendry, "Negative Refraction Makes a Perfect Lens," *Physical Review Letters*, vol. 85, no. 18, pp. 3966–3969, 2000.

[8] N. Seddon, "Observation of the Inverse Doppler Effect," *Science*, vol. 302, no. 5650, pp. 1537–1540, 2003.

[9] S. Kan, M. Sachan, J. Kirchhoff, and S. Majetich, "Crystallographic alignment of nanoparticles during self-assembly," *IEEE Transactions on Magnetics*, vol. 41, no. 10, pp. 3370–3372, 2005.

[10] S. Liu and T. J. Cui, "Concepts, Working Principles, and Applications of Coding and Programmable Metamaterials," *Advanced Optical Materials*, vol. 5, no. 22, pp. 601–627, 2017.

[11] W. Cai and V. M. Shalaev, *Optical metamaterials: fundamentals and applications*. New York: Springer, 2010.

[12] N. Fang, "Sub-Diffraction-Limited Optical Imaging with a Silver Superlens," *Science*, vol. 308, no. 5721, pp. 534–537, 2005.

[13] J. Li and C. T. Chan, "Double-negative acoustic metamaterial," *Physical Review E*, vol. 70, no. 5, pp. 11–14, 2004.

[14] Y. Wu, Y. Lai, and Z.-Q. Zhang, "Effective medium theory for elastic metamaterials in two dimensions," *Physical Review B*, vol. 76, no. 20, pp. 101–109, 2007.

[15] G. W. Milton and J. R. Willis, "On modifications of Newtons second law and linear continuum elastodynamics," *Proceedings of the Royal Society A: Mathematical, Physical and Engineering Sciences*, vol. 463, no. 2079, pp. 855–880, 2007.

[16] Y. Cheng, J. Y. Xu, and X. J. Liu, "One-dimensional structured ultrasonic metamaterials with simultaneously negative dynamic density and modulus," *Physical Review B*, vol. 77, no. 4, pp. 61–70, 2008.

[17] H. Huang, C. Sun, and G. Huang, "On the negative effective mass density in acoustic metamaterials," *International Journal of Engineering Science*, vol. 47, no. 4, pp. 610–617, 2009.

[18] P. A. Deymier, *Acoustic Metamaterials and Phononic Crystals*. Berlin, Heidelberg: Springer, 2013.
[19] *Acoustic metamaterials: negative refraction, imaging, lensing and cloaking*. Dordrecht: Springer, 2013.
[20] S. Yao, X. Zhou, and G. Hu, "Experimental study on negative effective mass in a 1D mass–spring system," *New Journal of Physics*, vol. 10, no. 4, pp. 72–83, 2008.
[21] H. H. Huang and C. T. Sun, "Anomalous wave propagation in a one-dimensional acoustic metamaterial having simultaneously negative mass density and Young's modulus," *The Journal of the Acoustical Society of America*, vol. 132, no. 4, pp. 2887–2895, 2012.
[22] X. N. Liu, G. K. Hu, G. L. Huang, and C. T. Sun, "An elastic metamaterial with simultaneously negative mass density and bulk modulus," *Applied Physics Letters*, vol. 98, no. 25, pp. 90–93, 2011.
[23] Mettler E, *Flugge (ed) Hanbook of Engineering Mechanics*, 1st ed. New York: McGraw-Hill, 1962.
[24] H. Huang, C. Sun, and G. Huang, "On the negative effective mass density in acoustic metamaterials," *International Journal of Engineering Science*, vol. 47, no. 4, pp. 610–617, 2009.
[25] Z. Liu, "Locally Resonant Sonic Materials," *Science*, vol. 289, no. 5485, pp. 1734–1736, 2000.
[26] R K. M. Ho, C. K. Cheng, Z. Yang, X. X. Zhang, and P. Sheng, "Broadband locally resonant sonic shields," *Applied Physics Letters*, vol. 83, no. 26, pp. 5566–5568, 2003.
[27] P. Sheng, X. Zhang, Z. Liu, and C. Chan, "Locally resonant sonic materials," *Physica B: Condensed Matter*, vol. 338, no. 1-4, pp. 201–205, 2003.
[28] H. Chen and C. T. Chan, "Acoustic cloaking in three dimensions using acoustic metamaterials," *Applied Physics Letters*, vol. 91, no. 18, pp. 111–113, 2007.
[29] H. Zhang, Y. Xiao, J. Wen, D. Yu, and X. Wen, "Flexural wave band gaps in metamaterial beams with membrane-type resonators: theory and experiment," *Journal of Physics D: Applied Physics*, vol. 48, no. 43, pp. 91–102, 2015.
[30] Salençon Jean, F. Romeo, and M. Ruzzene, *Wave Propagation in Linear and Nonlinear Periodic Media Analysis and Applications*. Vienna: Springer Vienna, 2013.
[31] D. Mead, "Free wave propagation in periodically supported, infinite beams," *Journal of Sound and Vibration*, vol. 11, no. 2, pp. 181–197, 1970.
[32] D. J. Mead, "Vibration Response and Wave Propagation in Periodic Structures," *Journal of Engineering for Industry*, vol. 93, no. 3, pp. 783–792, 1971.
[33] M. Faulkner and D. Hong, "Free vibrations of a mono-coupled periodic system," *Journal of Sound and Vibration*, vol. 99, no. 1, pp. 29–42, 1985.
[34] A. Krushynska, M. Miniaci, F. Bosia, and N. Pugno, "Coupling local resonance with Bragg band gaps in single-phase mechanical metamaterials," *Extreme Mechanics Letters*, vol. 12, pp. 30–36, 2017.
[35] L. Gavrić and G. Pavić, "A Finite Element Method for Computation of Structural Intensity by the Normal Mode Approach," *Journal of Sound and Vibration*, vol. 164, no. 1, pp. 29–43, 1993.

[36] G. Pavic, “The role of damping on energy and power in vibrating systems,” *Journal of Sound and Vibration*, vol. 281, no. 1-2, pp. 45–71, 2005.
[37] G. Pavić, “Structural surface intensity: An alternative approach in vibration analysis and diagnosis,” *Journal of Sound and Vibration*, vol. 115, no. 3, pp. 405–422, 1987.
[38] Alfredsson KS, Josefson BL, Wilson MA, “Use of the energy flow concept in vibration design,” *AIAA Journal*, vol. 34, no. 6, pp. 1250–1255, 1996.
[39] K. S. Alfredsson, “Active and Reactive Structural Energy Flow,” *Journal of Vibration and Acoustics*, vol. 119, no. 1, pp. 70–79, 1997.
[40] M. Chabchoub, S. Besset, and M. Ichchou, “Structural sources identification through an inverse mid-high frequency energy method,” *Mechanical Systems and Signal Processing*, vol. 25, no. 8, pp. 2948–2961, 2011.
[41] H. A. Babaa and M. Nouh, “An Investigation of Vibrational Power Flow in One-Dimensional Dissipative Phononic Structures,” *Journal of Vibration and Acoustics*, vol. 139, no. 2, pp. 211–210, 2017.
[42] P. F. Pai, “Metamaterial-based Broadband Elastic Wave Absorber,” *Journal of Intelligent Material Systems and Structures*, vol. 21, no. 5, pp. 517–528, 2010.
[43] Y. Xiao, J. Wen, and X. Wen, “Longitudinal wave band gaps in metamaterial-based elastic rods containing multi-degree-of-freedom resonators,” *New Journal of Physics*, vol. 14, no. 3, pp. 11–29, 2012.
[44] D. Yu, J. Wen, H. Zhao, Y. Liu, and X. Wen, “Flexural Vibration Band Gap in a Periodic Fluid-Conveying Pipe System Based on the Timoshenko Beam Theory,” *Journal of Vibration and Acoustics*, vol. 133, no. 1, pp. 126–129, 2011.
[45] J. Chen, B. Sharma, and C. Sun, “Dynamic behaviour of sandwich structure containing spring-mass resonators,” *Composite Structures*, vol. 93, no. 8, pp. 2120–2125, 2011.
[46] P. F. Pai, “Metamaterial-based Broadband Elastic Wave Absorber,” *Journal of Intelligent Material Systems and Structures*, vol. 21, no. 5, pp. 517–528, 2010.
[47] H. Peng and P. F. Pai, “Acoustic metamaterial plates for elastic wave absorption and structural vibration suppression,” *International Journal of Mechanical Sciences*, vol. 89, pp. 350–361, 2014.
[48] M. Nouh, O. Aldraihem, and A. Baz, “Wave propagation in metamaterial plates with periodic local resonances,” *Journal of Sound and Vibration*, vol. 341, pp. 53–73, 2015.
[49] G. Hu, L. Tang, A. Banerjee, and R. Das, “Metastructure With Piezoelectric Element for Simultaneous Vibration Suppression and Energy Harvesting,” *Journal of Vibration and Acoustics*, vol. 139, no. 1, pp. 54–65, 2016.
[50] K. K. Reichl and D. J. Inman, “Lumped mass model of a 1D metastructure for vibration suppression with no additional mass,” *Journal of Sound and Vibration*, vol. 403, pp. 75–89, 2017.
[51] A. Casalotti, S. El-Borgi, and W. Lacarbonara, “Metamaterial beam with embedded nonlinear vibration absorbers,” *International Journal of Non-Linear Mechanics*, vol. 98, pp. 32–42, 2018.
[52] J. Chen, B. Sharma, and C. Sun, “Dynamic behaviour of sandwich structure containing spring-mass resonators,” *Composite Structures*, vol. 93, no. 8, pp. 2120–2125, 2011.

[53] P. F. Pai, H. Peng, and S. Jiang, “Acoustic metamaterial beams based on multi-frequency vibration absorbers,” *International Journal of Mechanical Sciences*, vol. 79, pp. 195–205, 2014.

[54] A. Banerjee, E. P. Calius, and R. Das, “An impact based mass-in-mass unit as a building block of wideband nonlinear resonating metamaterial,” *International Journal of Non-Linear Mechanics*, vol. 101, pp. 8–15, 2018.

[55] R. L. Harne and D. C. Urbanek, “Enhancing Broadband Vibration Energy Suppression Using Local Buckling Modes in Constrained Metamaterials,” *Journal of Vibration and Acoustics*, vol. 139, no. 6, pp. 152–161, 2017.

[56] D. Maystre, S. Enoch, B. Gralak, and G. Tayeb, “Metamaterials: from microwaves to the visible region,” *Comptes Rendus Physique*, vol. 6, no. 6, pp. 693–701, 2005.

[57] E. P. Calius, X. Bremaud, B. Smith, and A. Hall, “Negative mass sound shielding structures: Early results,” *physica status solidi (b)*, vol. 246, no. 9, pp. 2089–2097, 2009.

[58] O. Abdeljaber, O. Avci, and D. J. Inman, “Optimization of chiral lattice based metastructures for broadband vibration suppression using genetic algorithms,” *Journal of Sound and Vibration*, vol. 369, pp. 50–62, 2016.

[59] T. Yu and G. A. Lesieutre, “Damping of Sandwich Panels via Acoustic Metamaterials,” *57th AIAA/ASCE/AHS/ASC Structures, Structural Dynamics, and Materials Conference*, 2016.

[60] C. Claeys, E. Deckers, B. Pluymers, and W. Desmet, “A lightweight vibro-acoustic metamaterial demonstrator: Numerical and experimental investigation,” *Mechanical Systems and Signal Processing*, vol. 70-71, pp. 853–880, 2016.

[61] T. Igusa and K. Xu, “Vibration Control Using Multiple Tuned Mass Dampers,” *Journal of Sound and Vibration*, vol. 175, no. 4, pp. 491–503, 1994.

[62] S. S. Rao, *Mechanical vibrations*. Upper Saddle River, NJ: Pearson Prentice Hall, 2011.

[63] W. Lacarbonara, *Nonlinear Structural Mechanics Theory, Dynamical Phenomena and Modeling*. Boston, MA: Springer US, 2013.

[64] V. Torczon, “On the Convergence of Pattern Search Algorithms,” *SIAM Journal on Optimization*, vol. 7, no. 1, pp. 1–25, 1997.

Vita

Ehab Emad Basta was born in 1994, in Al-Baha, Kingdom of Saudi Arabia. He received his primary education in Cairo, Egypt. He received his secondary education (I.G.C.S.E) in Fujairah, UAE. He received his B.Sc. degree in Mechanical Engineering from the American University of Sharjah in June 2017. In September 2017, he joined the Mechanical Engineering master's program at the American University of Sharjah as a graduate teaching assistant. His research interest is in nonlinear dynamics of vibrational structures.